AMERICAN SOCIETY FOR MICROBIOLOGY | Journal of Virology

Optimization of the Solubility of HIV-1-Neutralizing Antibody 10E8 through Somatic Variation and Structure-Based Design

Young D. Kwon,[a] Ivelin S. Georgiev,[a] Gilad Ofek,[a] Baoshan Zhang,[a] Mangaiarkarasi Asokan,[a] Robert T. Bailer,[a] Amy Bao,[a] William Caruso,[a] Xuejun Chen,[a] Misook Choe,[a] Aliaksandr Druz,[a] Sung-Youl Ko,[a] Mark K. Louder,[a] Krisha McKee,[a] Sijy O'Dell,[a] Amarendra Pegu,[a] Rebecca S. Rudicell,[a] Wei Shi,[a] Keyun Wang,[a] Yongping Yang,[a] Mandy Alger,[a] Michael F. Bender,[a] Kevin Carlton,[a] Jonathan W. Cooper,[a] Julie Blinn,[b,c] Joshua Eudailey,[b,c] Krissey Lloyd,[b,c] Robert Parks,[b,c] S. Munir Alam,[b,c] Barton F. Haynes,[b,c] Neal N. Padte,[d] Jian Yu,[d] David D. Ho,[d] Jinghe Huang,[e] Mark Connors,[e] Richard M. Schwartz,[a] John R. Mascola,[a] Peter D. Kwong[a]

Vaccine Research Center, National Institute of Allergy and Infectious Diseases, National Institutes of Health, Bethesda, Maryland, USA[a]; Duke Human Vaccine Institute, Departments of Medicine, Surgery, Pediatrics and Immunology, Duke University School of Medicine,[b] and Center for HIV/AIDS Vaccine Immunology-Immunogen Discovery, Duke University,[c] Durham, North Carolina, USA; The Aaron Diamond AIDS Research Center, Rockefeller University, New York, New York, USA[d]; HIV-Specific Immunity Section, Laboratory of Immunoregulation, National Institute of Allergy and Infectious Diseases, National Institutes of Health, Bethesda, Maryland, USA[e]

ABSTRACT

Extraordinary antibodies capable of near pan-neutralization of HIV-1 have been identified. One of the broadest is antibody 10E8, which recognizes the membrane-proximal external region (MPER) of the HIV-1 envelope and neutralizes >95% of circulating HIV-1 strains. If delivered passively, 10E8 might serve to prevent or treat HIV-1 infection. Antibody 10E8, however, is markedly less soluble than other antibodies. Here, we describe the use of both structural biology and somatic variation to develop optimized versions of 10E8 with increased solubility. From the structure of 10E8, we identified a prominent hydrophobic patch; reversion of four hydrophobic residues in this patch to their hydrophilic germ line counterparts resulted in an ~10-fold decrease in turbidity. We also used somatic variants of 10E8, identified previously by next-generation sequencing, to optimize heavy and light chains; this process yielded several improved variants. Of these, variant 10E8v4 with 26 changes versus the parent 10E8 was the most soluble, with a paratope we showed crystallographically to be virtually identical to that of 10E8, a potency on a panel of 200 HIV-1 isolates also similar to that of 10E8, and a half-life in rhesus macaques of ~10 days. An anomaly in 10E8v4 size exclusion chromatography that appeared to be related to conformational isomerization was resolved by engineering an interchain disulfide. Thus, by combining a structure-based approach with natural variation in potency and solubility from the 10E8 lineage, we successfully created variants of 10E8 which retained the potency and extraordinary neutralization breadth of the parent 10E8 but with substantially increased solubility.

IMPORTANCE

Antibody 10E8 could be used to prevent HIV-1 infection, if manufactured and delivered economically. It suffers, however, from issues of solubility, which impede manufacturing. We hypothesized that the physical characteristic of 10E8 could be improved through rational design, without compromising breadth and potency. We used structural biology to identify hydrophobic patches on 10E8, which did not appear to be involved in 10E8 function. Reversion of hydrophobic residues in these patches to their hydrophilic germ line counterparts increased solubility. Next, clues from somatic variants of 10E8, identified by next-generation sequencing, were incorporated. A combination of structure-based design and somatic variant optimization led to 10E8v4, with substantially improved solubility and similar potency compared to the parent 10E8. The cocrystal structure of antibody 10E8v4 with its HIV-1 epitope was highly similar to that with the parent 10E8, despite 26 alterations in sequence and substantially improved solubility. Antibody 10E8v4 may be suitable for manufacturing.

Over the last 5 years, extraordinary antibodies capable of effectively neutralizing human immunodeficiency virus type 1 (HIV-1) have been identified (1–9). In addition to serving as potential templates for an antibody-based HIV-1 vaccine, the passive delivery of these antibodies could be used to prevent HIV-1 infection or to treat those infected with HIV-1 therapeutically (10–13).

Such passive use of antibodies, however, would require their economical manufacturing and delivery, and HIV-1-neutralizing antibodies often have characteristics which make their manufacture less than optimal. Antibody 10E8, which targets the membrane-proximal external region (MPER) of the gp41 subunit (14, 15), is one of these: it neutralizes 98% of a panel of 181 diverse HIV-1 isolates (14). Despite this extraordinary breadth, its poor solubility impedes manufacturing. Other MPER antibodies, such as 2F5 and 4E10 (8, 16–18), however, have greater solubility, sug-

Received 28 December 2015 **Accepted** 29 March 2016

Accepted manuscript posted online 6 April 2016

Citation Kwon YD, Georgiev IS, Ofek G, Zhang B, Asokan M, Bailer RT, Bao A, Caruso W, Chen X, Choe M, Druz A, Ko S-Y, Louder MK, McKee K, O'Dell S, Pegu A, Rudicell RS, Shi W, Wang K, Yang Y, Alger M, Bender MF, Carlton K, Cooper JW, Blinn J, Eudailey J, Lloyd K, Parks R, Alam SM, Haynes BF, Padte NN, Yu J, Ho DD, Huang J, Connors M, Schwartz RM, Mascola JR, Kwong PD. 2016. Optimization of the solubility of HIV-1-neutralizing antibody 10E8 through somatic variation and structure-based design. J Virol 90:5899–5914. doi:10.1128/JVI.03246-15.

Editor: W. I. Sundquist, University of Utah

Address correspondence to John R. Mascola, jmascola@mail.nih.gov, or Peter D. Kwong, pdkwong@nih.gov.

Supplemental material for this article may be found at http://dx.doi.org/10.1128/JVI.03246-15.

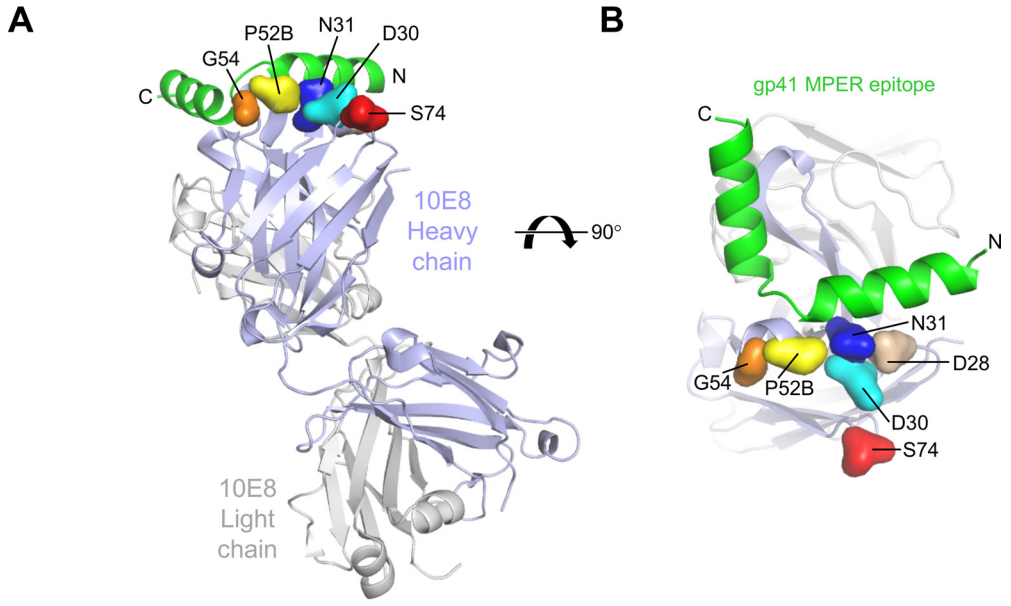

C

	IC50					IC80				
Heavy chain	**BaL.01**	**JRFL.JB**	**REJO.67**	**QH0515.01**	**THRO.18**	**BaL.01**	**JRFL.JB**	**REJO.67**	**QH0515.01**	**THRO.18**
D28W	0.6	0.6	0.6	0.2	0.2	0.2	0.4	0.2	0.4	0.2
D30W	0.4	0.7	1.0	1.0	0.2	0.4	0.5	0.5	0.5	0.3
N31W	0.9	1.1	1.8	2.8	0.4	0.4	0.7	0.9	0.9	0.4
P52BW	0.5	0.4	0.6	0.9	0.1	0.2	0.3	0.2	0.3	0.2
G54W	0.6	0.6	0.6	0.6	0.3	0.3	0.5	0.3	0.2	0.4
S74W	0.3	0.2	0.4	0.6	0.2	0.2	0.3	0.2	0.3	0.2
D28W,G54W	0.5	0.5	1.3	2.2	0.2	0.2	0.4	0.3	0.4	0.2
D30W, G54W	0.9	0.7	0.6	0.7	0.2	0.3	0.4	0.2	0.6	0.2
N31W, G54W	0.8	0.6	0.4	1.0	0.2	0.4	0.5	0.2	0.4	0.3
P52BW, G54W	0.6	0.5	0.7	1.3	0.2	0.3	0.5	0.4	0.5	0.3
D28W, D30W	1.3	1.1	4.5	3.4	0.6	0.5	0.8	1.1	1.0	0.5
D28W, N31W	2.4	1.2	1.4	0.4	0.8	0.8	0.6	1.1	1.0	0.5
D30W, N31F	0.6	0.6	0.3	0.1	0.3	0.3	0.5	0.2	0.4	0.3

>3-fold increase in IC50 or IC80 (Loss of function) >3-fold decrease in IC50 or IC80 (Gain of fuction)

D

Antibody (μg/ml)	**100.00**	**33.33**	**11.11**	**3.70**	**1.23**	**0.41**
10E8H/L	0.0543	0.0536	0.0494	0.0507	0.0483	0.0488
10E8-HC6/L	0.1652	0.0774	0.0684	0.0479	0.0453	0.045
10E8-HC6-S74W/L	0.4521	0.1341	0.0805	0.0547	0.0486	0.0445
4E10				2.0728	1.8094	1.3546
Synagis	0.0477	0.0468	0.0469	0.0532	0.0462	0.0444

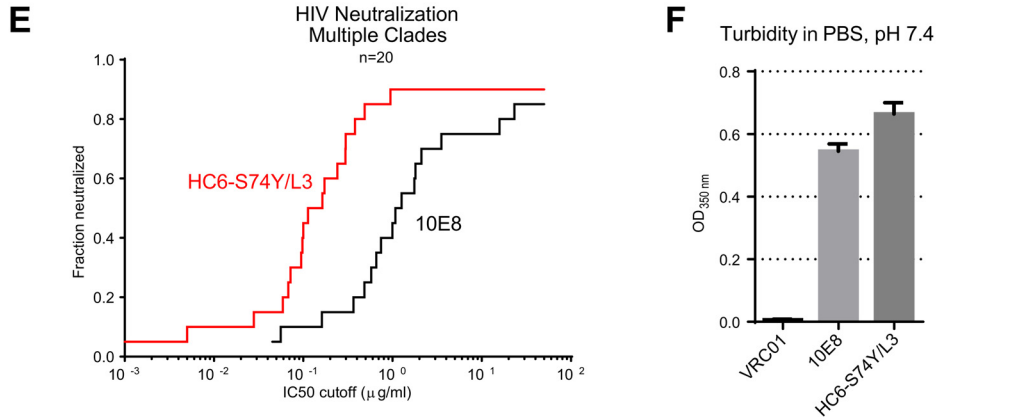

FIG 1 Epitope recognition, HIV-1 neutralization, polyreactivity, and turbidity of 10E8 variants with alterations of coplanar paratope residues. (A) Fab 10E8 is shown in ribbon representation, with the MPER epitope in red and coplanar residues with the epitope highlighted. (B) Ninety-degree view of coplanar residues selected for alteration to tryptophan. (C) Effect of single and double tryptophan/phenylalanine substitutions on neutralization. Numbers represent the ratio of the IC_{50} or IC_{80} of variants to that of 10E8. (D) Cardiolipin binding assay with 4E10 and palivizumab (Synagis) as positive and negative controls, respectively; polyreactive binding based on an ELISA criterion of being three times the background (0.18 OD at 450 nm) is indicated by yellow highlighting. (E) Breadth and potency assessed on a panel of 20 HIV-1 isolates. (F) Turbidity of antibody 10E8 and HC6-S74Y/L3 variant.

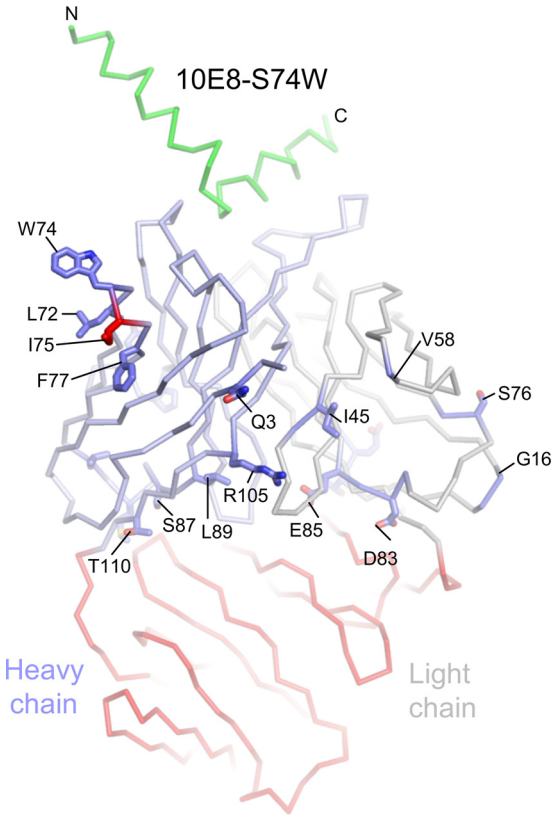

FIG 2 Cocrystal structure of 10E8 S74W in complex with HIV-1 MPER. The variable domain is shown in C_α-backbone representation in light blue. All residues were superimposed with the parent 10E8 within a Cα RMSD of 1Å, except for the Cα of residue Ile75 (in red) in the heavy chain. Cα distances of all residues between the parent 10E8 in the constant domain were greater than 1Å and are colored in red. Residues that are different from the 10E8v4 structure described in Fig. 10 are labeled.

gesting that the poor solubility of 10E8 is not intrinsic to its function and could be improved.

Here we use a combination of structural biology and somatic variant optimization to improve the solubility of antibody 10E8. We hypothesized that the reduced solubility of antibody 10E8 reflected the aggregation of hydrophobic surfaces. From the structure of 10E8, we identified hydrophobic patches, which did not appear to be required for function, and reverted residues in these patches to their hydrophilic germ line counterparts. Similarly we identified somatic variants which were more soluble but less potent than the parent 10E8. In these variants, we tested somatic alterations in the mature 10E8 that appeared to be of functional relevance by altering residues in more soluble but less potent variants to their counterparts in the somatically mature 10E8. Overall, we created several variants (see Table S1 in the supplemental material) with increased solubility, all of which showed no polyreactivity and retained the breadth and potency of the parent 10E8. Of these, antibody 10E8v4 appeared to be the most soluble, and we determined its cocrystal structure with its MPER epitope. We also characterized the polyreactivity of 10E8v4, its bioavailability in mice and rhesus macaques, and its behavior on size exclusion chromatography (SEC). An anomaly in SEC behavior appeared to be related to slow conformational isomerization, so we engineered a disulfide linking the heavy and light chains of 10E8 to resolve this issue. Our findings show how a combination of structural biology and somatic variant optimization can be used to improve the manufacturing characteristics of an antibody, with 10E8v4 or its disulfide-locked variant potentially suitable for manufacturing.

MATERIALS AND METHODS

Antibody expression and purification. Mammalian codon-optimized genes encoding either an antibody heavy chain or a light chain were synthesized and cloned into mammalian expression vector pVRC8400 (VRC, NIAID, Bethesda, MD). For small-scale preparation, 50 μg of antibody heavy chain DNAs and 50 μg of light chain plasmid DNAs were combined in 5 ml of Opti-MEM medium (Invitrogen, CA) and then mixed with 5 ml of transfection medium containing 0.27 ml of ExpiFectamine 293 transfection reagent (Invitrogen, CA) in Opti-MEM medium. The complex of DNAs and ExpiFectamine 293 transfection reagent was incubated for 20 min at room temperature before being mixed with 80 ml of Expi 293S cell culture (2.5×10^6 cells/ml) in a 250-ml shaking flask. The transfected cell culture was returned to suspension incubation for 24 h at 37°C, 8% CO_2, and 125 rpm and then fed with 10 ml of the antibody expression enhancement medium Ab Boost (ABI, VA). Six days posttransfection, the supernatant was harvested by centrifugation and filtered through 0.22-μm filters. The antibody IgG was captured by an affinity column of protein A (protein A plus agarose; Thermo Scientific, Rockford, IL) and further purified by a size exclusion column (Superdex 200; GE Healthcare). Pu-

TABLE 1 Crystallographic data and refinement

Parameter	Value[a] for: 10E8-S74W–MPER complex	10E8v4-MPER complex
Data collection statistics		
Space group	$C222_1$	$P2_12_12_1$
Cell dimensions		
a, *b*, *c* (Å)	135.76, 189.25, 71.72	65.02, 79.52, 211.36
α, β, γ (°)	90, 90, 90	90, 90, 90
Resolution (Å)	50–3.29 (3.35–3.29)	50–2.40 (2.49–2.40)
R_{sym}	0.12 (0.59)	0.10 (0.46)
R_{pim}	0.042 (0.242)	0.073 (0.334)
CC1/2	0.983 (0.920)	0.956 (0.873)
$I/\sigma I$	19.4 (2.7)	9.3 (2.2)
Completeness (%)	98.8 (86.9)	87.3 (91.1)
Redundancy	9.1 (5.1)	2.6 (2.5)
Refinement statistics		
Resolution (Å)	37.5–3.29	36.4–2.40
No. of reflections	14,140	38,241
R_{work}/R_{free}	23.0/28.3	19.0/23.6
No. of atoms		
Protein	3,640	6,986
Water	0	357
B-factors (Å^2)		
Protein	138.2	41.4
Water		42.8
Ramachandran plot		
Favored regions (%)	92.92	96.85
Allowed regions (%)	7.08	3.15
Disallowed regions (%)	0	0
RMSD		
Bond length (Å)	0.005	0.003
Bond angle (°)	0.697	0.535
PDB ID	5IQ7	5IQ9

[a] Numbers in parentheses are for the highest-resolution shell.

TABLE 2 Anti-cardiolipin antibody-binding properties of 10E8 HC6/L3 variants with alterations at position 74[a]

μg/ml	HC6-S74A/ L3	HC6-S74D/ L3	HC6-S74E/ L3	HC6-S74F/ L3	HC6-S74H/ L3	HC6-S74I/ L3	HC6-S74K/ L3	HC6-S74L/ L3	HC6-S74M/ L3
10.00	0.088	0.059	0.066	0.147	0.232	0.144	0.148	0.185	0.124
3.33	0.047	0.041	0.046	0.067	0.082	0.063	0.060	0.069	0.059
1.11	0.046	0.042	0.046	0.050	0.063	0.054	0.064	0.056	0.047
0.37	0.043	0.036	0.045	0.041	0.041	0.040	0.047	0.039	0.036

μg/ml	HC6-S74N/ L3	HC6-S74P/ L3	HC6-S74Q/ L3	HC6-S74R/ L3	HC6-S74T/ L3	HC6-S74V/ L3	HC6-S74Y/ L3	HC6-S74/ L3	10E8 WT
10.00	0.131	0.084	0.117	0.104	0.094	0.123	0.143	0.068	0.038
3.33	0.061	0.051	0.053	0.053	0.046	0.054	0.059	0.043	0.038
1.11	0.051	0.040	0.043	0.044	0.043	0.045	0.047	0.044	0.038
0.37	0.038	0.046	0.038	0.043	0.041	0.047	0.043	0.041	0.041

Autoreactive controls:						
Pos	0.662	0.658	0.722	0.7146	**Pos avg=**	**0.689**
Neg	0.038	0.040	0.040	0.0425	**Neg avg=**	**0.040**

[a] Values in the far left column are the concentrations of the 10E8 variants. Values in the table body are ELISA OD_{450} results from cardiolipin binding, with yellow and green highlighting intermediate autoreactive.

rified antibodies were dialyzed against 1× phosphate-buffered saline (PBS), and characterized with SDS-PAGE.

Structure-based engineering of antibody 10E8 variants. (i) Identification of hydrophobic patches. To identify hydrophobic patches, we used the DSSP program (19) to calculate the solvent-accessible surface area (SASA) for each antibody residue. Hydrophobic residues with SASAs of more than 20 $Å^2$ that were not part of the known paratope and that were not deemed to be essential for the stability of the paratope, the heavy chain-light chain interface, or other antibody structural elements were selected for further analysis. Candidate mutations were identified using the OSPREY protein design suite of programs (20), as well as from next-generation sequencing (NGS) data.

(ii) Identification of functionally important somatically altered residues. To identify regions of 10E8 that were somatically altered and important for neutralization, we aligned sequences of more potently neutralizing somatic variants with those of less potently neutralizing variants, selected residues that were in close proximity to the MPER epitope, and if different, swapped the corresponding residues in combination (e.g., single, double, triple, or quadruple mutations), and then tested the neutralization potency against a nine-virus panel. The nine-virus panel was selected to include strains representing (i) the spectrum of neutralization sensitivity to wild-type 10E8 and (ii) diverse HIV-1 clades.

(iii) Creation of a disulfide-locked CDR H3. To create a disulfide-locked heavy-chain third-complementarity-determining region (CDR H3), we examined the gp41 MPER peptide-bound 10E8v4 Fab structure and identified the Cα of Tyr100e (this corresponds to insert "e" at position 100 in Kabat numbering) in the CDR H3 region of the heavy chain and the Cα of Ser30 in the light chain as being separated by 5.8 Å, close to the optimal Cα-Cα distance for a disulfide bond. Therefore, we replaced these residues with cysteines to form a disulfide bond.

Nomenclature of designs. Sequences for structure-based designs are shown in Table S1 in the supplemental material. The nomenclature is as follows: HC6-S74Y, somatic variant heavy chain HC6 with S74Y mutation; HC6-S74Y-DKTT, heavy chain HC6-S74Y with L72D, I75K, F77T, and M84T mutations; H6-DTKT, somatic variant heavy chain H6 with L72D, S74T, I75K, and F77T mutations; H6-DTKT-DNTY, heavy chain H6-DTKT with N28D, D31N, S52T, and H98Y mutations; H8-DYKT, somatic variant heavy chain H8 with L72D, S74Y, I75K, and F77T mutations; L3-ASPAKQ, somatic variant light chain L3 with S1A, Y2S, T8P, G9A, G16K, and R17Q mutations; 10E8v1, heavy chain HC6-S74Y-DKTT plus light chain L3; 10E8v4, heavy chain H6-DTKT-DNTY plus light chain L3-ASPAKQ; 10E8v5, heavy chain HC6-S74Y-DKTT plus light chain L3-ASPAKQ.

Assessment of antibody-mediated neutralization of HIV-1. Neutralization was measured using single-round-of-infection HIV-1 Env pseudoviruses and TZM-bl target cells, as described previously (21). Neutralization curves were fit by nonlinear regression using a five-parameter Hill slope equation. The 50% and 80% inhibitory concentrations (IC_{50} and IC_{80}) were reported as the antibody concentrations required to inhibit infection by 50% and 80%, respectively.

Assessments of solubility. To measure the turbidity of 10E8 variants in PBS, each variant in IgG elution buffer (pH 2.8; Thermo Scientific, Rockford, IL) was subjected to buffer exchange by either direct dilution with PBS or dialysis in PBS. For the direct dilution method, we concentrated antibodies in IgG elution buffer to 10 optical densities (OD) at 280 nm, diluted them 20-fold with PBS, and incubated them overnight at room temperature; we then loaded 90 μl of the diluent onto a 96-well microplate (Corning, NY) and measured the absorbance at 350 nm using a SPECTRAmax PLUS 384 spectrophotometer (Molecular Devices, Sunnyvale, CA). For the dialysis method, 1 ml of 10E8 variants (1 OD at 280 nm, in elution buffer, pH 2.8; Thermo Scientific) was dialyzed against 1× PBS overnight at 20°C using a Slide-A-Lyzer dialysis cassette (10,000 molecular weight cutoff; Thermo Scientific). The contents of the dialysis bag were resuspended thoroughly by pipetting up and down, 90 μl of the contents was loaded onto a 96-well microplate, and absorbance was measured at 350 nm. As a control, the elution buffer was diluted 20-fold with PBS or dialyzed in PBS.

Kinetic concentration. Three milliliters of 10E8 variant (0.35 OD at 280 nm) in PBS was centrifuged at 4,000 × *g* for 20 min using Amicon Ultra-4 centrifugal filter units (30,000 nominal molecular weight limit; EMD Millipore). Prior to concentration, the 10E8 variants were first passed through a 0.22-μm filter to remove aggregates. The concentrated volume of each variant after centrifugation was measured by weighing it, and its concentration was measured at 280 nm using NanoDrop technology (Thermo Scientific, Rockford, IL).

DLS. Dynamic light scattering (DLS) measurements were performed at 25°C using a DynaPro Plate Reader II (Wyatt Technology, Santa Barbara, CA). The samples were dialyzed with 1× PBS, adjusted to 0.5 mg/ml, and filtered with 0.22-μm filters prior to analysis. The data were analyzed using DYNAMICS version 7.1.7 software (Wyatt Technology).

Assessment of antibody polyreactivity. Antibodies were assessed for autoreactivity on two platforms: antinuclear antibodies by staining on HEp2 cells (Zeus Scientific catalog no. FA2400; ANA HEp2 test system) and anti-cardiolipin ELISA (Inova Diagnostics catalog no. 708625; QUANTA Lite ACA IgG III) per the manufacturers' instructions. On HEp2 cells, antibodies were tested at 50 and 25 μg/ml. Control antibodies VRC01-LS, 4E10, and VRC07-G54W were included in

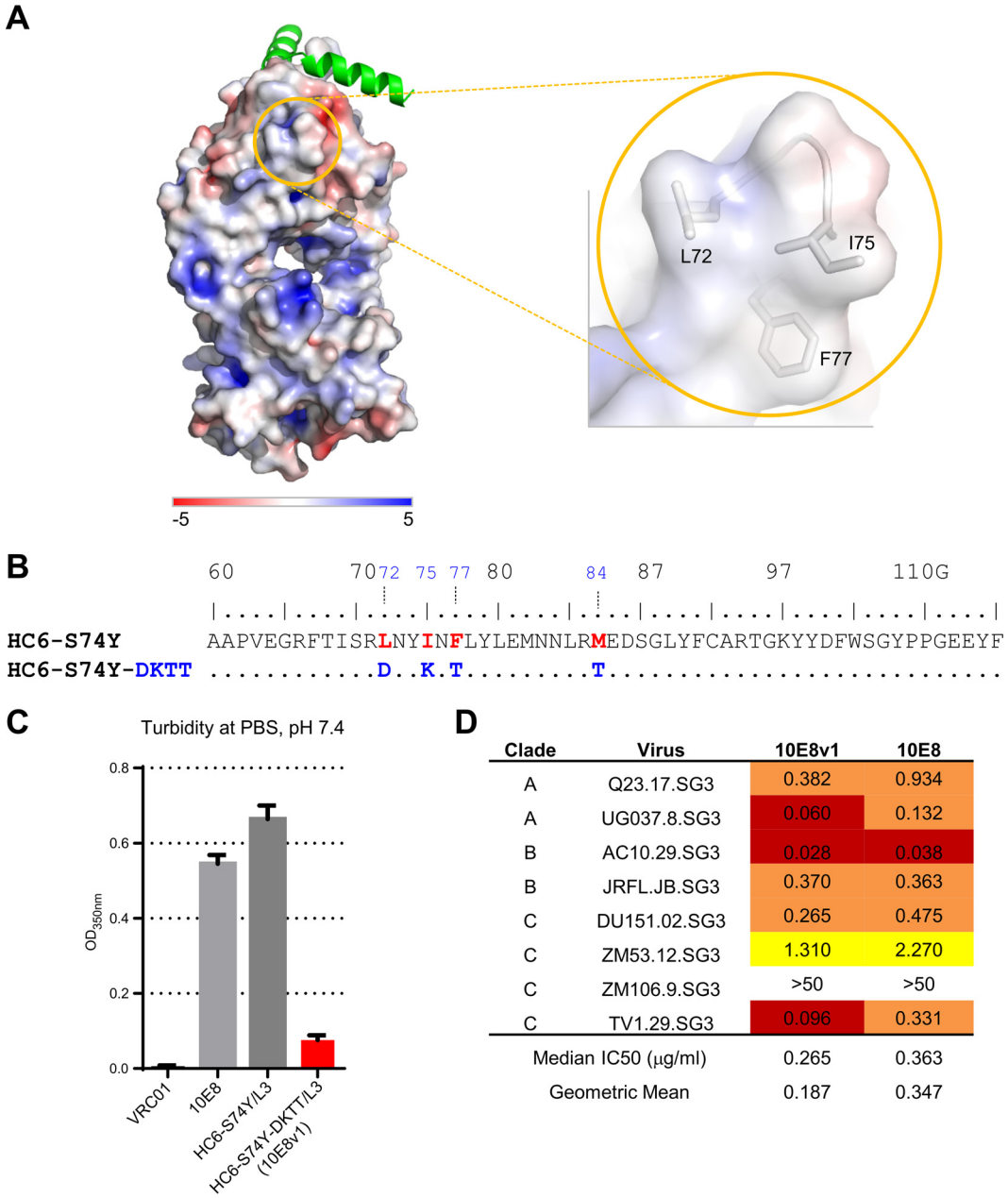

Clade	Virus	10E8v1	10E8
A	Q23.17.SG3	0.382	0.934
A	UG037.8.SG3	0.060	0.132
B	AC10.29.SG3	0.028	0.038
B	JRFL.JB.SG3	0.370	0.363
C	DU151.02.SG3	0.265	0.475
C	ZM53.12.SG3	1.310	2.270
C	ZM106.9.SG3	>50	>50
C	TV1.29.SG3	0.096	0.331
Median IC50 (μg/ml)		0.265	0.363
Geometric Mean		0.187	0.347

FIG 3 Reversion to germ line of hydrophobic residues in the framework region 3 of the 10E8 heavy chain variant (HC6-S74Y) enhances solubility. (A) Fab 10E8 in surface representation, with colors indicating electrostatic potential: red, electronegative; blue, electropositive; white, hydrophobic. A hydrophobic patch is formed by Leu72, Ile75, and Phe77. (B) Alteration of four hydrophobic residues to their germ line counterparts to create heavy chain variant 10E8v1. Sequences are shown based on the Kabat numbering scheme. (C) Turbidity of 10E8v1. (D) Neutralization potency of 10E8v1 versus the wild type.

each slide and assigned a score between 0 and 3+. Test antibodies that scored greater than 1+ at 25 μg/ml were considered autoreactive. In the cardiolipin binding assay, monoclonal antibodies (MAbs) that scored greater than three times the background at 33 μg/ml were considered autoreactive.

Assessment of bioavailability in mice. BALB/c mice were divided into three groups containing three mice per group, and the mice in each group were administered intraperitoneally 100 μg of 10E8, 10E8v4, or 10E8v5 antibody. Blood was drawn from all animals at 1, 2, 4, 7, and 10 days after antibody administration, and serum was isolated and analyzed for levels of antibody in individual mice. Costar 96-well enzyme immunoassay/radioimmunoassay plates (Corning, NY) were coated with 100 ng per well of goat anti-human IgG Fc-γ fragment (Jackson ImmunoResearch) overnight at 4°C. The plates were washed three times with PBS plus Tween and blocked with PBS containing 5% milk and 0.5% bovine serum albumin (BSA) for 2 h at room temperature. Mouse serum from the treated animals and purified 10E8, 10E8v4, or 10E8v5 MAb in PBS for the standard curves were added to the wells in 1:2 serial dilutions in PBS containing 2% milk and 0.2% BSA and incubated for 2 h. After washing, peroxidase-conjugated goat anti-human IgG (Jackson ImmunoResearch) was incubated for 1 h at room temperature. Samples were detected by a TMB (3,3′,5,5′-tetramethylbenzidine) liquid substrate system (Sigma), and spectrophotometric readings were performed at 450 nm. All animals were bred

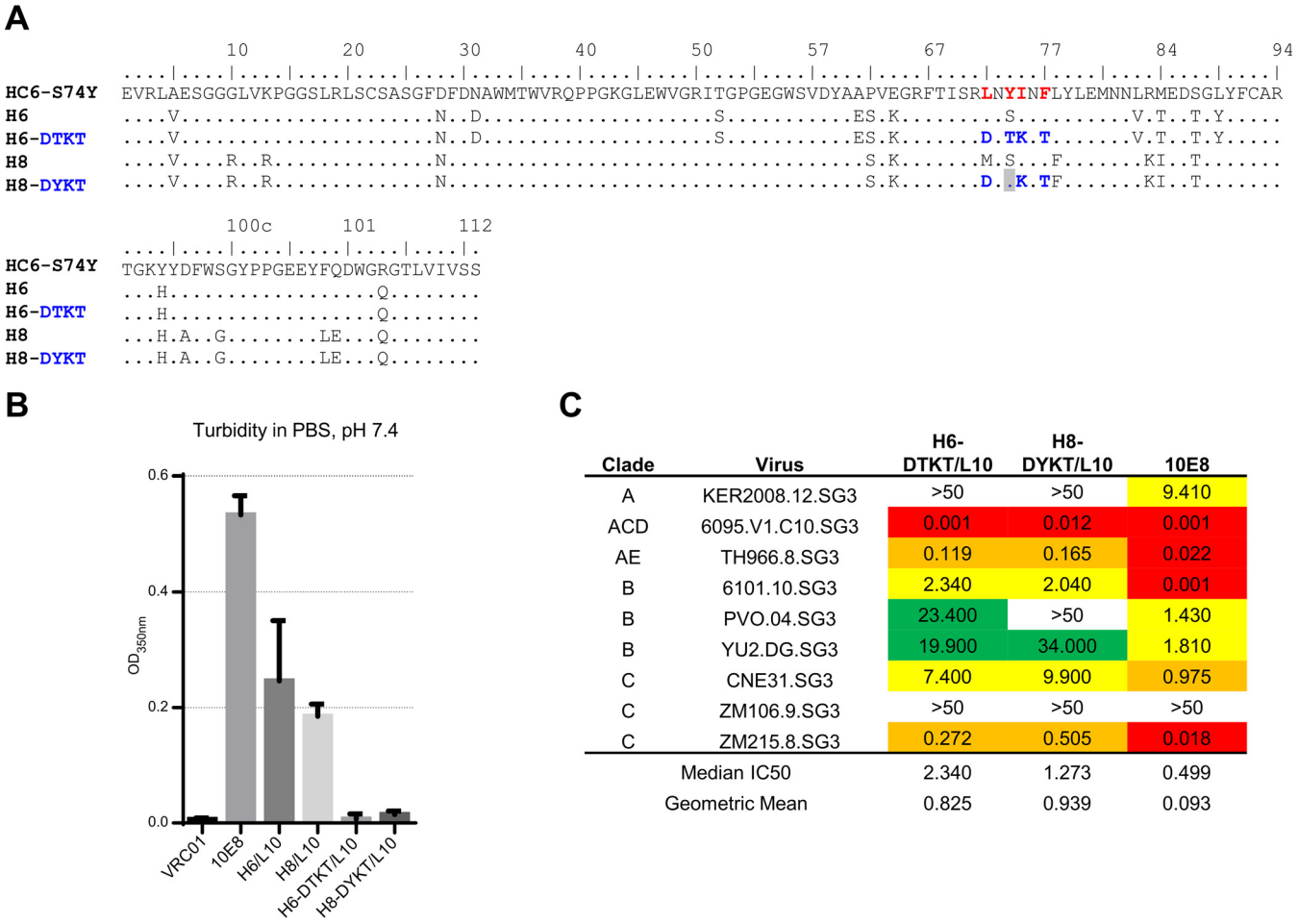

Clade	Virus	H6-DTKT/L10	H8-DYKT/L10	10E8
A	KER2008.12.SG3	>50	>50	9.410
ACD	6095.V1.C10.SG3	0.001	0.012	0.001
AE	TH966.8.SG3	0.119	0.165	0.022
B	6101.10.SG3	2.340	2.040	0.001
B	PVO.04.SG3	23.400	>50	1.430
B	YU2.DG.SG3	19.900	34.000	1.810
C	CNE31.SG3	7.400	9.900	0.975
C	ZM106.9.SG3	>50	>50	>50
C	ZM215.8.SG3	0.272	0.505	0.018
	Median IC50	2.340	1.273	0.499
	Geometric Mean	0.825	0.939	0.093

FIG 4 Somatic 10E8 variants showed increased solubility but reduced potency versus 10E8. (A) Sequences of 10E8 and somatic variants (residues in red indicate reversion to germ line); (B) turbidity; (C) neutralization potency.

and maintained at the Comparative Bioscience Center of The Rockefeller University in accordance with the regulations of its Institutional Animal Committee Care and Use Committee (IACUC). All animal studies were conducted under protocols approved by this committee.

Assessment of bioavailability in rhesus macaques. Rhesus macaques of Indian origin were administered low-endotoxin antibody preparations (<1 endotoxin unit [EU]/mg) intravenously at 10 mg of Ab/kg of body weight. Whole-blood samples were collected prior to injection and at multiple time points until week 4 after administration. Antibody concentrations in serum were measured by ELISA as described previously (22), with the exception that plates were coated with 200 ng/well of MPER peptide. Pharmacokinetic parameters were calculated in WinNonlin Software using the two-compartment model.

Crystallization, structure determination, and refinement. Purified 10E8-S74W Fab in buffer containing 5 mM Tris-HCl, pH 7.5, 150 mM NaCl, and 0.02% NaN_3 was complexed to an MPER peptide composed of gp41 residues 656 to 683 flanked by terminal solubility tags (RRR_{656}NEQELLELDKWASLWNWFDITNWLWYIR_{683}RRR) in a 1:3 protein-to-peptide molar ratio, concentrated to ~10 mg/ml, and set up in vapor diffusion hanging-drop crystallizations using the same conditions that were used to obtain the 10E8 wild-type (WT) MPER crystal structure: 40% polyethylene glycol (PEG) 400, 0.1 M Na citrate, 0.1 M Tris (pH 7.5). Purified 10E8v4 Fab in buffer containing 5 mM Tris-HCl, pH 7.5, 150 mM NaCl, and 0.02% NaN_3 was also complexed to the same MPER peptide composed of gp41 residues 656 to 683 flanked by terminal solubility tags (RRR_{656}NEQELLELDKWASLWNWFDITNWLWYIR_{683}RRR) in a 1:3 protein-to-peptide molar ratio. This complex was set up in crystallization screens composed of 576 initial conditions adapted from the commercially available Hampton (Hampton Research), Precipitant Synergy (23), and Wizard Classic (Rigaku) screens using a Honeybee 963 robot. Crystallizations were set up at 20°C using vapor diffusion hanging drops, and trays were imaged with a Rockimager (Formulatrix). Crystal hits were hand optimized with additive screens (Hampton Research). X-ray diffraction data were collected at the Advanced Photon Source, using insertion device 22, and extended to 2.4-Å resolution for crystals grown in a condition composed of 25% isopropanol, 15% PEG 3350, 0.1 M Tris (pH 8.5), and 10% Jeffamine (Hampton Research). Data were processed using HKL-2000 (24), and the structures were solved with molecular replacement using the parent 10E8 structure as a search model (PDB ID 4G6F) in Phaser (25). Refinement of the structures was undertaken with Phenix (26), with iterative model building in Coot (27). All graphics were prepared with PyMOL (PyMOL Molecular Graphics System).

Time-resolved size exclusion chromatography. A 2× PBS mobile phase was prepared with a 4:1 (vol/vol) dilution of water (JT Baker catalog no. 9831-03) and 10× PBS (Lonza catalog no. 17-517Q). The solution was stored in a 1-liter polyethylene terephthalate glycol modified (PETG) Biotainer bottle at room temperature. Fifty microliters (3.8 mg/ml) of 10E8v4 was injected onto the Acquity BEH SEC column (P/N, 186005225; 4.6- by 150-mm inside diameter; particle size, 1.7 μm; pore size, 20 nm) of

A

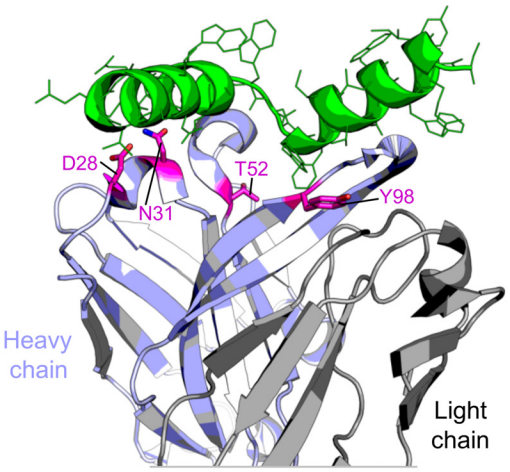

B

```
                    10        20        30        40        50        57        67        77        84        94
                    ....|....|....|....|....|....|....|....|....|....|....|....|....|....|....|....|....|....|
HC6-S74Y            EVRLAESGGGLVKPGGSLRLSCSASGFDFDNAWMTWVRQPPGKGLEWVGRITGPGEGWSVDYAAPVEGRFTISRLNYINFLYLEMNNLRMEDSGLYFCAR
H6-DTKT             ....V.....................N..D.....................S...........ES.K.......D.TK.T.......V.T..T.Y.....
H6-DTKT-DNTY        ....V.....................N..D.....................S...........ES.K.......D.TK.T.......V.T..T.Y.....

                    100c      101       112
                    ....|....|....|....|....|.
HC6-S74Y            TGKYYDFWSGYPPGEEYFQDWGRGTLVIVSS
H6-DTKT             ...H.................Q........
H6-DTKT-DNTY        ...N.................Q........
```

C

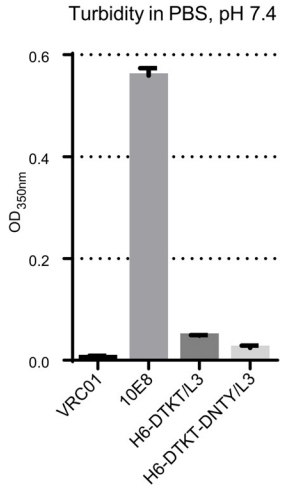

D

Clade	Virus	H6-DTKT/L3	H6-DTKT-DNTY/L3	10E8
A	KER2008.12.SG3	>50	>50	>25
ACD	6095.V1.C10.SG3	0.001	0.001	0.003
AE	TH966.8.SG3	0.023	0.013	0.033
B	6101.10.SG3	0.069	0.016	0.032
B	PVO.04.SG3	1.720	0.943	1.900
B	YU2.DG.SG3	3.200	2.040	2.800
C	CNE31.SG3	1.990	1.680	1.730
C	ZM106.9.SG3	>50	>50	>25
C	ZM215.8.SG3	0.030	0.018	0.036
Median IC50 (μg/ml)		0.069	0.018	0.036
Geometric Mean		0.125	0.072	0.140

FIG 5 Swaps of variant heavy chain residues proximal to epitope and pairing with L3 light chain enhanced neutralization potency. (A) Structure of 10E8 highlighting location of residues altered to improve potency; (B) sequence of 10E8 heavy chain variants and alterations to improve potency; (C) turbidity of the variants in PBS; (D) neutralization potency.

the Waters Acquity UPLC H-class system consisting of a sample manager-FTN (model code SDI), a quaternary solvent manager (model code QSM), and a tunable UV detector (model code TUV). An isocratic, 2× PBS mobile phase (pH 7.4) was run at a flow rate of 0.4 ml/min for 8 min. UV absorbance was detected at 280 nm using Empower 3 software. Three distinct fractions were isolated and collected by hand, in 1.7-ml microcentrifuge tubes, at the outlet end of the flow path immediately following the UV detector. Fraction collection times were estimated by visual inspection, using a historical data set to approximate when the peaks would elute. For this study, three fractions were isolated (F1, ~3 to 3.3 min; F2, ~3.9 to 4.3 min, and F3, ~5.8 to 6.4 min). Upon collection, 50 μl of each fraction was reinjected back onto the column within a 30-min time frame from elution ($t = 0$) for confirmation of the fractionated peaks. The remaining aliquot of each fraction was stored at 4°C for 22 h. At $t = 22$ h, 50 μl of fractions 1, 2, and 3 were separately reinjected onto the column, and chromatograms for $t = 0$ and $t = 22$ were compared for each fraction.

Accession numbers. Atomic coordinate and structure factors for 10E8-S74W in complex with HIV-1 gp41 MPER and for 10E8v4 in complex with HIV-1 gp41 MPER have been deposited in the Protein Data Bank under accession numbers 5IQ7 and 5IQ9, respectively. Sequences for10E8 variants have been deposited in GenBank under accession numbers KU951246 to KU951253.

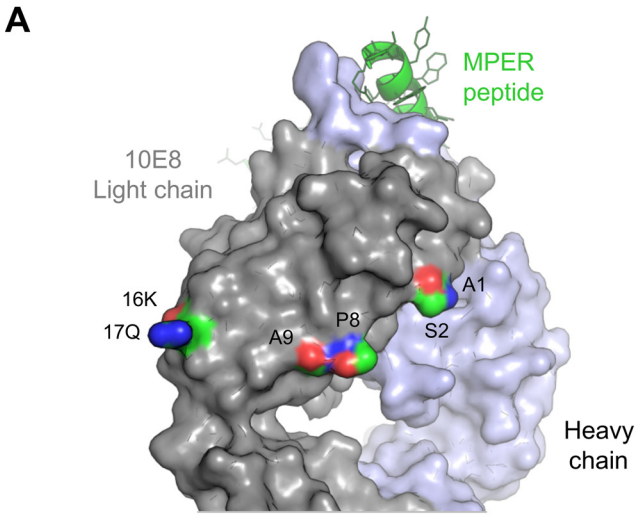

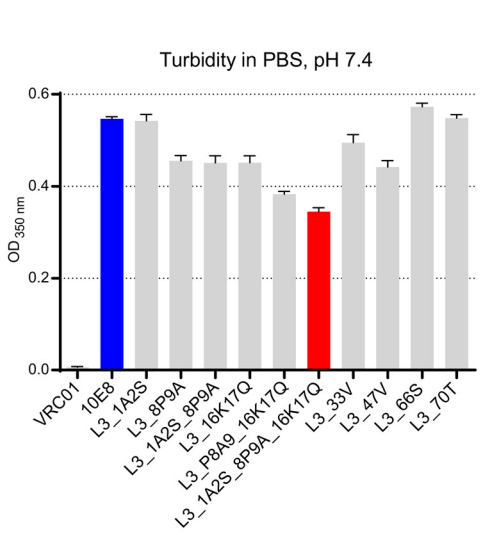

B

```
                  11        21        31        41        51        61        71        81        91        98
                  ....|....|....|....|....|....|....|....|....|....|....|....|....|....|....|....|....|....|
L3                SYELTQDTGVSVALGRTVTITCRGDSLRSHYASWYQKKPGQAPVLLFYGKNNRPSGIPDRFSGSASGNRASLTITGAQAEDEADYYCSSRDKSGSRLSVF
L10               AS.....PA.....KQ..............V.............V.................S...T.....A......D..................
L3_ASPAKQ         AS.....PA.....KQ.....................................................................................
```

D

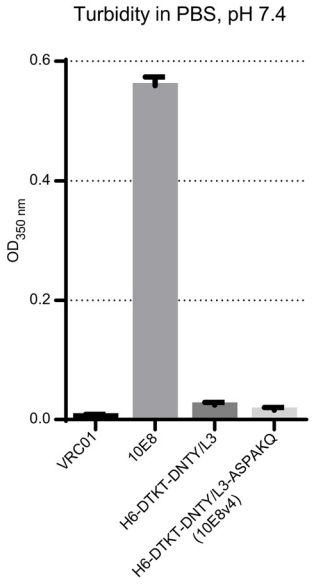

E

Clade	Virus	H6-DTKT-DNTY/L3	10E8v4	10E8
A	KER2008.12.SG3	>50	>50	>25
ACD	6095.V1.C10.SG3	0.001	0.001	0.003
AE	TH966.8.SG3	0.013	0.020	0.033
B	6101.10.SG3	0.016	0.025	0.032
B	PVO.04.SG3	0.943	1.100	1.900
B	YU2.DG.SG3	2.040	2.030	2.800
C	CNE31.SG3	1.680	1.080	1.730
C	ZM106.9.SG3	>50	>50	>25
C	ZM215.8.SG3	0.018	0.015	0.036
Median IC_{50} (μg/ml)		0.018	0.025	0.036
Geometric Mean		0.072	0.073	0.140

FIG 6 Swaps of variant light chain residues further improved solubility. (A) Structure of 10E8 highlighting location of residues altered to improve potency; (B) sequence of 10E8 light chain variants and alterations to improve solubility; (C and D) turbidity of 10E8 light chain variants; (E) neutralization potency.

RESULTS

Initial attempts to optimize 10E8 suggested solubility to be a critical limiting factor. We and others previously showed MPER-directed antibodies to recognize epitopes comprising not only the MPER, but also the hydrophobic viral membrane itself (28–35). To improve the function of antibody 10E8, we first asked whether replacement by Trp of surface-exposed 10E8 residues coplanar with the MPER would enhance neutralization (Fig. 1A and B; see Table S1 in the supplemental material). A number of substitutions increased potency, although generally in an isolate-specific fashion (Fig. 1C). A Ser74Trp substitution in the 10E8 heavy chain, however, showed a general increase in potency, both in 50% inhibitory concentration (IC_{50}) and in 80% inhibitory concentration (IC_{80}) (Fig. 1C), and the crystal structure of 10E8-S74W confirmed that 74W did not interact with MPER (Fig. 2 and Table 1). Once we identified that the Ser74Trp mutation increased potency, we introduced this mutation to a somatic heavy chain variant named HC6 (see Table S1), which neutralized the select viruses

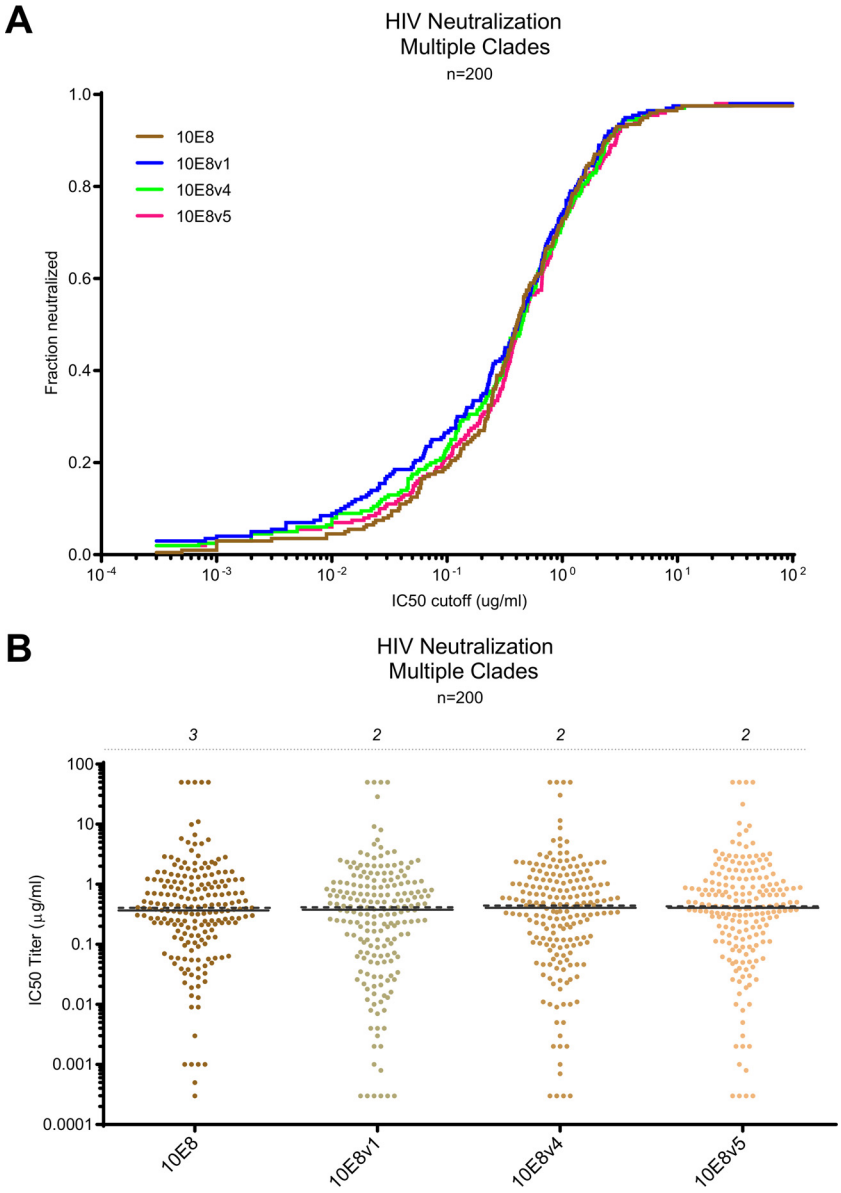

FIG 7 10E8v1, 10E8v4, and 10E8v5 retain extraordinary breadth and potency of the parent 10E8. (A) Breadth-potency curve for a panel of 200 HIV-1 isolates; (B) aggregate IC_{50}s (the percentage of viruses resistant to neutralization [$IC_{50} > 50$ μg/ml] is shown at the top of each column).

more potently than the parent 10E8 when paired with a somatic light chain variant named L3 (see Table S1) (36).

Characterization of the cardiolipin-binding properties of the HC6-Ser74Trp variant of 10E8, however, indicated potential polyreactivity (Fig. 1D). We substituted all 18 other amino acids at position 74 and assessed the polyreactivity. A Ser74Tyr variant was observed not to be polyreactive (Table 2) while retaining increased potency (Fig. 1E). Turbidity measurements, however, of protein A-eluted antibody in PBS, pH 7.4, indicated the Ser74Tyr variant of 10E8 to be even less soluble than the wild-type 10E8 (Fig. 1F). Together, these results indicated that prior to attempting to enhance potency, it might be best to increase 10E8 solubility.

Enhancement of solubility through alteration of a hydrophobic surface patch and use of somatic variants. To increase the solubility of 10E8 and its variants, we searched for hydrophobic surface patches. A number of such patches were observed, and the largest of these included the heavy-chain third-complementarity-determining region (CDR H3), which showed extensive interactions with the MPER. We did not alter this patch, as its hydrophobicity was likely related to MPER recognition and therefore critical for function. However, a second hydrophobic patch comprising Leu72, Ile75, and Phe77 in the framework region 3 of the heavy chain was spatially separated from the MPER (Fig. 3A), and we tested the effect of reverting these three residues as well as Met84 (which displayed a large SASA) to their germ line counterparts (Fig. 3B); we paired this 4-reverted-residue heavy chain, named HC6-S74Y-DKTT, with the L3 light chain and named the variant 10E8v1. Assessment of the turbidity of 10E8v1 indicated an ~10-fold decrease (Fig. 3C), while assessment of the neutralization po-

TABLE 3 Neutralization of 10E8 variants on a 200-or 203-isolate panel[a]

10E8 or variant	Total no. of viruses in panel	No. of viruses neutralized at IC_{50} (IC_{80}) of:					% of viruses neutralized at IC_{50} (IC_{80}) of:					Median IC_{50} (IC_{80})	Geometric mean IC_{50} (IC_{80})
		<50 μg/ml	<10 μg/ml	<1 μg/ml	<0.1 μg/ml	<0.01 μg/ml	<50 μg/ml	<10 μg/ml	<1 μg/ml	<0.1 μg/ml	<0.01 μg/ml		
10E8	200	195 (195)	194 (186)	145 (57)	38 (9)	9 (5)	98 (98)	97 (93)	73 (29)	19 (5)	5 (3)	0.392 (1.76)	0.315 (1.52)
10E8v1	200	196 (195)	195 (190)	148 (57)	53 (15)	17 (6)	98 (98)	98 (95)	74 (29)	27 (8)	9 (3)	0.397 (2.03)	0.228 (1.42)
10E8v4	200	196 (195)	194 (181)	143 (49)	46 (11)	13 (5)	98 (98)	97 (91)	72 (25)	23 (6)	7 (3)	0.435 (2.50)	0.276 (1.94)
10E8v5	200	196 (195)	194 (185)	146 (51)	42 (11)	12 (6)	98 (98)	97 (93)	73 (26)	21 (6)	6 (3)	0.418 (2.07)	0.307 (1.70)
10E8v4	203	198 (198)	198 (185)	146 (54)	39 (10)	11 (3)	98 (98)	98 (91)	72 (27)	19 (5)	5 (1)	0.428 (2.23)	0.329 (1.67)
10E8v4-DS	203	171 (146)	148 (125)	93 (40)	29 (7)	11 (3)	84 (72)	73 (62)	46 (20)	14 (3)	5 (1)	0.706 (2.41)	0.641 (2.06)

[a] Numbers in parentheses are results for IC_{80}.

tency of 10E8v1 indicated an ~2-fold increase on an eight-isolate panel (Fig. 3D).

We had previously identified somatic variants of 10E8 by next-generation sequencing (NGS) of B cell transcripts of donor N152, the source of antibody 10E8. Three of the heavy chain-light chain mixtures lacked polyreactivity (37). These variants, derived from heavy chains H6_dN152 and H8_dN152 (these heavy chains are termed H6 and H8 throughout this paper), both retained the hydrophobic framework region 3 patch (Fig. 4A). We tested the turbidity of the two 10E8 variants, and when paired with light chain L10, both H6/L10 and H8/L10 showed less than half the turbidity of the wild-type 10E8 (Fig. 4B). We reverted the framework region 3 hydrophobic patch in both H6 and H8, expressed the resulting antibody variants, and tested their turbidity. We observed that the H6-reverted (H6-DTKT)/L10 and H8-reverted (H8-DYKT)/L10 had substantially improved turbidity, approaching the level observed for antibody VRC01 (Fig. 4B). However, the neutralization potency for both H6-DTKT/L10 and H8-DYKT/L10 was almost 10-fold weaker than that of wild-type 10E8 (Fig. 4C). Thus, while somatic variants and reversion to germ line assisted in reducing solubility, the somatic variants were often of substantially lower potency.

Enhancement of potency through transplantation of paratope-proximal alterations of 10E8. We focused on improving the potency of H6-reverted (H6-DTKT)/L10 and analyzed positions in the H6 heavy chain which differed from the more potent HC6-S74Y. We observed four changes in close proximity to the MPER, at residues 28, 31, 52, and 98 (Fig. 5A), and altered the sequence of the H6-reverted heavy chain to that of their HC6-S74Y counterparts at these four positions (Fig. 5B). We also observed the L3 light chain to have increased neutralization potency in comparison to the L10 light chain and the combination of H6 with L3 not to be polyreactive and therefore created variants with alterations at residues 28, 31, 52, and 98 (H6-DTKT-DNTY) of the H6-reverted heavy chain (H6-DTKT) with the L3 light chain. The turbidity of these H6/L3-optimized variants remained substantially lower than that of the parent 10E8 (Fig. 5C). Moreover, on a nine-isolate panel, these 10E8 variants exceeded the neutralization potency of the parent 10E8 (Fig. 5D).

We further analyzed the sequence of L3 for differences from L10 (Fig. 6A and B). We created a series of variants in which these residues were altered individually or in combination and characterized the turbidity of these variants (Fig. 6C). Alteration of six residues at the N terminus of the light chain resulted in the lowest turbidity (Fig. 6C and D) with retained potency (Fig. 6E). We paired the residue 28-, 31-, 52-, and 98-altered variant (H6-DTKT-DNTY) of the H6-reverted heavy chain (H6-DTKT) with the 6-residue-altered L3 light chain (L3-ASPAKQ) and named the variant 10E8v4. We also paired the HC6-S74Y-DKTT heavy chain with the 10E8v4 light chain (L3-ASPAKQ) and named this variant 10E8v5.

Characteristics of 10E8v1, 10E8v4, and 10E8v5. We assessed the neutralization of 10E8v1, 10E8v4, and 10E8v5 on a panel of 200 diverse HIV-1 isolates. Overall, the neutralization of these three 10E8 variants recapitulated well the extraordinary breadth and potency of the parent 10E8 (Fig. 7A). While 10E8v1 was slightly more potent than the others at a lower concentration, overall the neutralization breadth-potency curves were extremely similar, as were the overall IC_{50}s (Fig. 7A and B and Table 3).

We also assessed the solubility of these 10E8 variants. In the turbidity assay, 10E8v1 was the least soluble, whereas 10E8v4 and 10E8v5 were of comparable solubilities (Fig. 8A and B). We also tested the ease by which antibody could be concentrated, through the use of a kinetic concentration assay, whereby 3 ml of 10E8 or 10E8 variant at 0.35 optical density (OD) at 280 nm was placed over an Amicon Ultra-4 centrifugal filter unit (EMD Millipore) and centrifuged for 20 min at 4,000 × *g*. By this "ease-of-concentration" assay, 10E8v4 concentrated the most easily, 10E8v5 the next most easily, and 10E8v1 similarly to the parent 10E8 (Fig. 8C). We also used dynamic light scattering to analyze the particle size distribution and polydispersity of the 10E8 variants. While the parent 10E8 displayed polydisperse characteristics, 10E8v1, 10E8v4, and 10E8v5 all appeared monodisperse (Fig. 8D).

When analyzed for HEp2 cell reactivity, neither the parent 10E8 nor the three 10E8 variants showed reactivity at 50 or 25 μg/ml (Fig. 9A). 10E8 and all three variants were also negative on cardiolipin (Fig. 9B) (we note that Chen and colleagues did observe 10E8 to bind cardiolipin [29], a difference that likely reflects differences in cardiolipin preparations). When analyzed in a mouse intraperitoneal infusion model, both 10E8v4 and 10E8v5 showed increased bioavailability compared to the parent 10E8 (Fig. 9C). When dosed at 10 mg/kg in a rhesus macaque intravenous infusion model, 10E8v4 showed a substantial increase in bioavailability, with an estimated half-life of ~10 days, roughly twice that of the parent 10E8 (~5 days) (Fig. 9D). When we added the LS mutation (see Table S1 in the supplemental material), which has been reported to extend antibody serum half-life by improving affinity for the neonatal Fc receptor (FcRn) (38, 39), to 10E8v4, we observed an additional increase in half-life (Fig. 9D). Together, the results indicate 10E8v4 to be substantially more soluble than the parent 10E8, with substantially increased half-life.

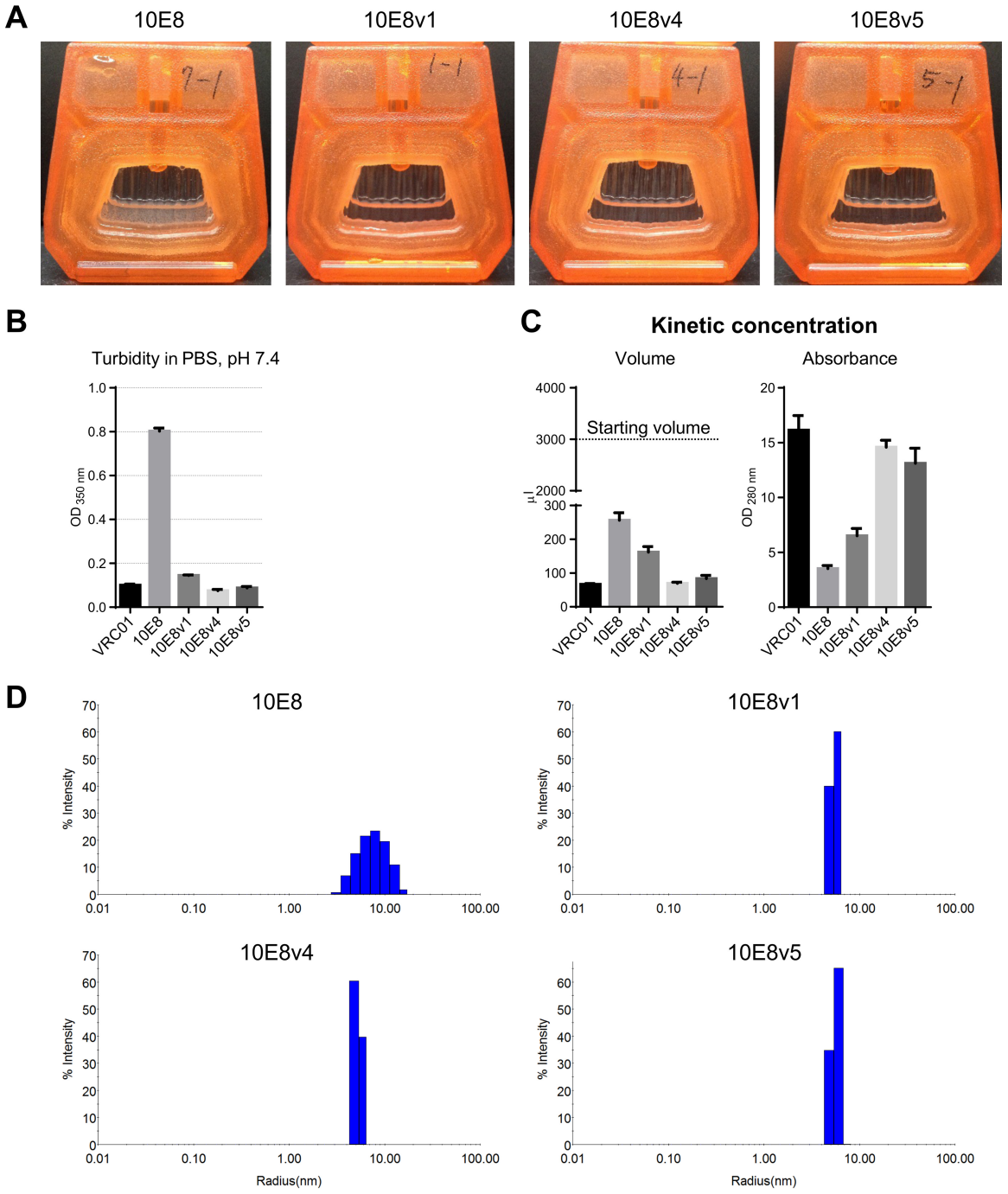

FIG 8 10E8v1, 10E8v4, and 10E8v5 are soluble and monodisperse. (A) Solubility of 10E8 and 10E8 variants after dialysis in PBS, pH 7.4; (B) turbidity in PBS; (C) kinetic concentration assay, with the volume after centrifugation (left) and the absorbance at 280 nm (right); (D) dynamic light scattering indicating 10E8 to be polydispersed, whereas 10E8v1, 10E8v4, and 10E8v5 were monodispersed.

Crystal structure of 10E8v4 with MPER peptide. To provide a characterization of 10E8v4 at the atomic level, we determined its crystal structure in complex with an MPER peptide (Fig. 10). Despite 26 alterations, the variable domain of the 10E8v4 structure was virtually identical to that of the parent 10E8. Specifically, the average Cα root mean square deviation (RMSD) was 0.52 Å, and the 10E8v4 paratope structure was even more highly preserved, with a Cα RMSD of 0.12 Å. Interestingly, the first helical region of the 10E8 epitope in the parent 10E8 structure (MPER residues 656 to 669) was mostly disordered in the 10E8v4 structure, consistent with differences observed in this helix in the two asymmetric unit complexes of the parent 10E8 structure (14) as well as the PGT151-soluble micelle context (15). In contrast, the C-terminal MPER helix was substantially ordered in the 10E8v4 structure, with clear electron density from residue 670 through residue 683. Within these ordered

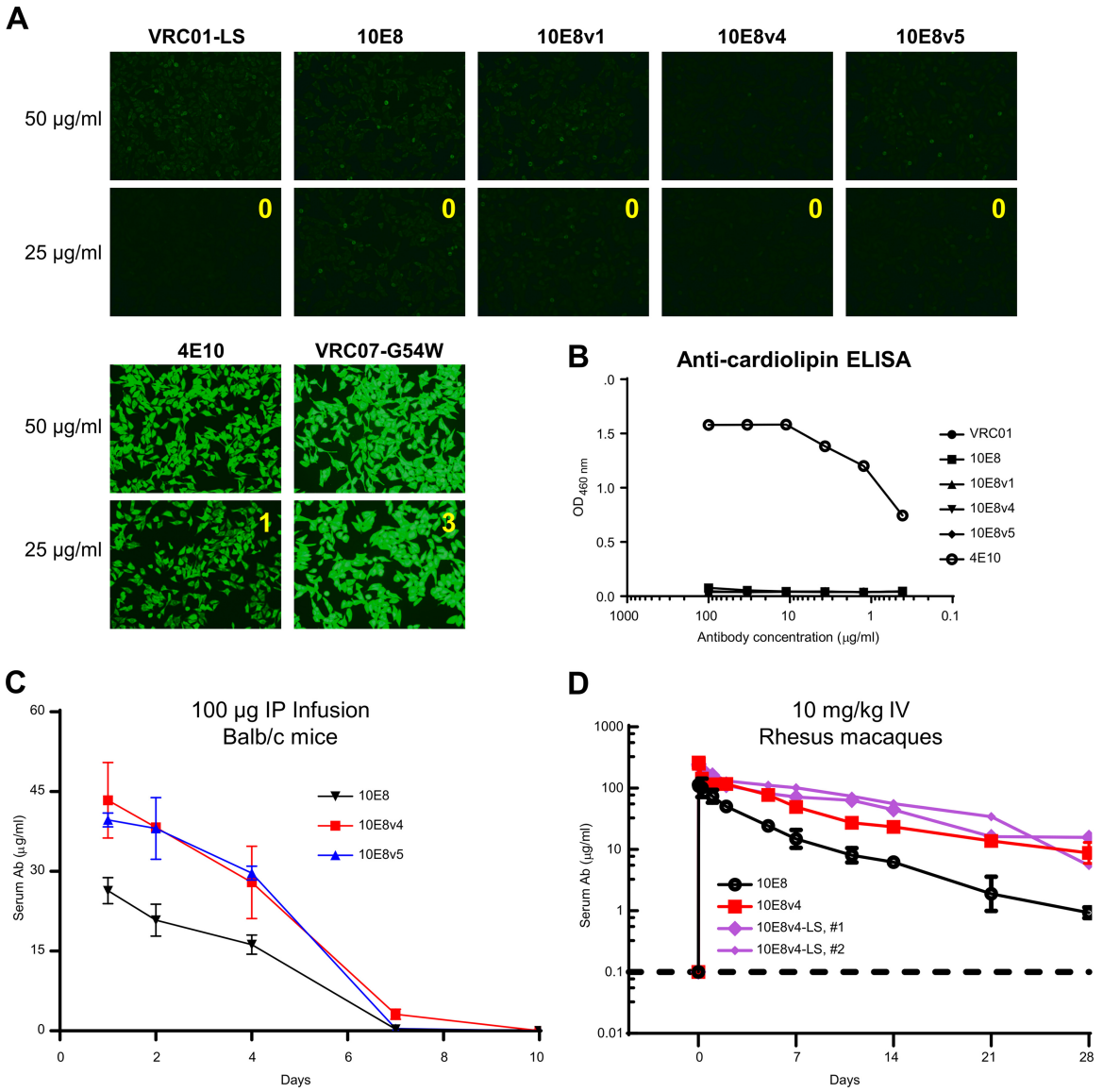

FIG 9 10E8v1, 10E8v4, and 10E8v5 showed no polyreactivity, with increased bioavailability in mice and macaques for 10E8v4 and 10E8v4-LS. (A) HEp2 cell staining assays on 10E8 variants. (B) Anti-cardiolipin ELISA. (C) BALB/c mice were divided into groups of three, and the mice in each group were administered intraperitoneally (IP) 100 µg of 10E8, 10E8v4, or 10E8v5 antibody on day 0. The serum antibody levels shown are the mean values for each group of mice, and error bars indicate standard deviations. (D) Serum antibody level assessment for rhesus macaques. IV, intravenous. "LS" indicates alteration of the heavy chain to increase affinity for neonatal Fc receptor.

residues, an RMSD of 0.17 Å was observed relative to the MPER in the parent 10E8 structure. Together, the structural characteristics reveal 10E8v4 to have the same overall structure and direct MPER interactions as the parent 10E8, despite 26 alterations in sequence.

Slow conformational isomerization of the 10E8v4 paratope and its disulfide fixation. Analytical size exclusion chromatography revealed 10E8v4 to elute as three peaks (Fig. 11A, top chromatogram). If any of the three peaks (F1 to F3) was pooled and immediately assessed again by size exclusion chromatography, the elution profile was characterized by a single peak, skewed toward the position of the original peak (Fig. 11A, bottom left chromatograms). However, if each of the three peaks was allowed after separation to incubate at 4°C for 22 h, then rerunning each of these equilibrated peaks resulted in the same three original peaks (Fig. 11A, bottom right chromatograms).

The dramatic difference in chromatograms between an immediately run sample and an equilibrated sample suggests slow conformational isomerization as a likely mechanism. Because each of the peaks gave a similar molecular weight when analyzed by size exclusion chromatography with multiangle light scattering (SEC-MALS) (Fig. 11B), the difference in size exclusion mobility likely related to different degrees of hydrophobic interaction with the matrix. The most hydrophobic portion of the structure was the CDR H3, which suggested slow conformational isomerization of the CDR H3 (which contained a diproline motif) as the likely source of the multiple size exclusion chromatography peaks. To test this idea, we analyzed the CDR H3 region of the 10E8v4

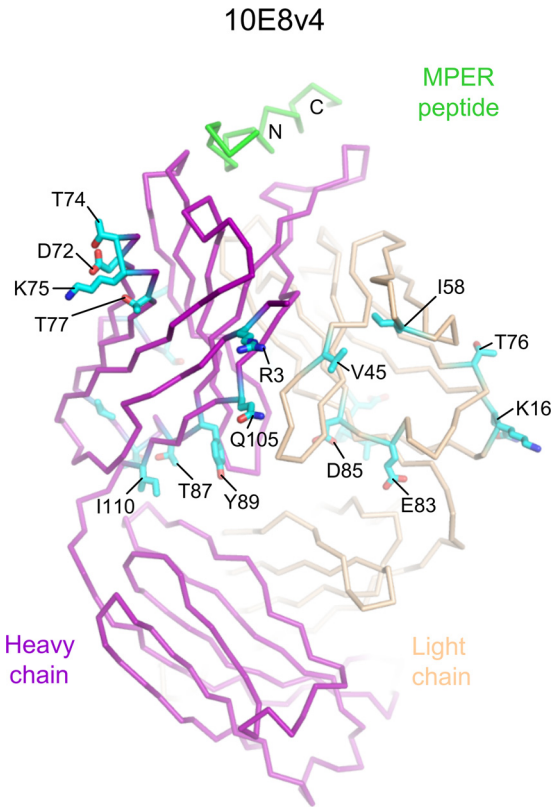

FIG 10 Cocrystal structure of 10E8v4 in complex with HIV-1 MPER. Residues that differ between 10E8v4 and the parent 10E8 are highlighted in stick representation, labeled, and colored cyan.

structure for residues which could accommodate an introduced disulfide to lock the CDR H3 in place. Modeling suggested Tyr100e in the CDR H3 and Ser30 in the light chain to be close to optimal for disulfide formation, and we created this interchain 100eC-30C double cysteine variant (10E8v4-DS) (Fig. 11D). Comparison of the 10E8v4-DS mutant on SDS-PAGE under reducing and nonreducing conditions indicated the near 100% formation of an interchain disulfide, with the 10E8v4-DS variant neutralizing HIV-1 being less potent than 10E8v4 (Fig. 11C and Table 3). Notably, when we analyzed the 10E8v4-DS mutant by size exclusion chromatography, we observed it to elute as a single dominant peak (Fig. 11E).

DISCUSSION

With its near pan-neutralization of HIV-1, antibody 10E8 overcomes one of the most challenging aspects of neutralizing HIV-1, its diversity. Moreover, assessment of its protective capacity in rhesus macaques (40) demonstrates protection from simian-human immunodeficiency virus (SHIV) BalP4 challenge at a similar dose as antibody VRC01 (0.3 mg/kg), despite 10E8 having an IC_{80} that is ~100-fold lower than that of VRC01 against SHIV BalP4 in the TZM-bl assay. These highly positive qualities of antibody 10E8 were, however, offset by its less than optimal solubility. Here we show how a combination of structure-based design and incorporation of natural variation from somatic variants of the 10E8 lineage provides a means to increase solubility, without sacrificing breadth or potency.

Because biological molecules are complex, with mobile surface residues, complicated domain isomerizations, and heuristic temperature-dependent behaviors, their solubility is more than can be described by a single number delineating a maximum concentration in a physiological buffer. For example, we could concentrate antibody 10E8 to over 10 mg/ml; however, once a small amount of 10E8 precipitated, additional precipitate tended to accumulate until a substantial portion of the antibody was no longer in solution. Similarly, we observed accumulating 10E8 precipitate to occur at 4°C, with substantially higher solubility at 37°C. Moreover, when antibody 10E8 was eluted from a protein A column at pH 2.8 and brought to neutral pH, a substantial amount of precipitate often formed. Such precipitation can substantially impede manufacturability.

To improve the solubility of antibody 10E8, we chose to measure a step closely linked to a common manufacturing step (transitioning from pH 2.8 to neutral pH) with an easy-to-measure readout (turbidity or the absorbance of the solution at 350 nm). For a control, we used antibody VRC01, which we had previously manufactured and formulated at 100 mg/ml (41, 42). By mutational alteration of hydrophobic surface patches and incorporation of specific residues found in somatic variants with higher solubility, we succeeded in engineering a 10E8 variant with turbidity similar to that of antibody VRC01 (Fig. 4B). The most soluble variants unfortunately showed reduced potency, but we did succeed in creating 10E8v4, which has potency and breadth nearly indistinguishable from that of the parent 10E8 (Fig. 7); 10E8v4 behaved in turbidity assessments and kinetic concentration assays comparably to antibody VRC01 (Fig. 8).

The near doubling of half-life in the rhesus macaque from the ~5 days for the parent 10E8 to ~10 days for 10E8v4 was an unanticipated bonus. Was this a lucky coincidence? While turbidity generally does not correlate well with half-life (e.g., the half-lives of antibodies 10E8 and VRC01 are similar despite the latter having much lower turbidity), within each lineage there did appear to be modest correlation. As turbidity is much easier to measure than antibody half-life, a potential correlation even with only some lineages may be worth further investigation.

Broad HIV-1-neutralizing antibodies generally arise in highly diverse lineages with substantial somatic hypermutation (43); for example, the lineage of antibody VRC01 comprises at least four clades with sequence differences that could exceed 50% (44). Such lineage diversity provides a pool of somatic variants with distinct biological characteristics. Structure-based design, meanwhile, provides both a functional context and the ability to stitch diverse alterations gleaned from divergent lineage variants into an improved chimera. We previously used a mixture of somatic variation and structure-based optimization to improve the potency of antibody VRC01, and specifically to create the chimeric improved antibody VRC07-523 (22). Here we used similar methodologies, but instead of potency, we focused on improving antibody solubility. Whether with potency, as with VRC07-523-LS, or with solubility, as with 10E8v4, overall the results demonstrate the power of coupling rational design with somatic variation to improve selected traits of a target antibody. Of the variants obtained, both 10E8v4 and 10E8v4-DS are potentially of interest for manufacture. We note that if the slow conformational isomerization of 10E8v4 is not an issue for licensure, then it may be preferred because of its higher potency; other considerations include the

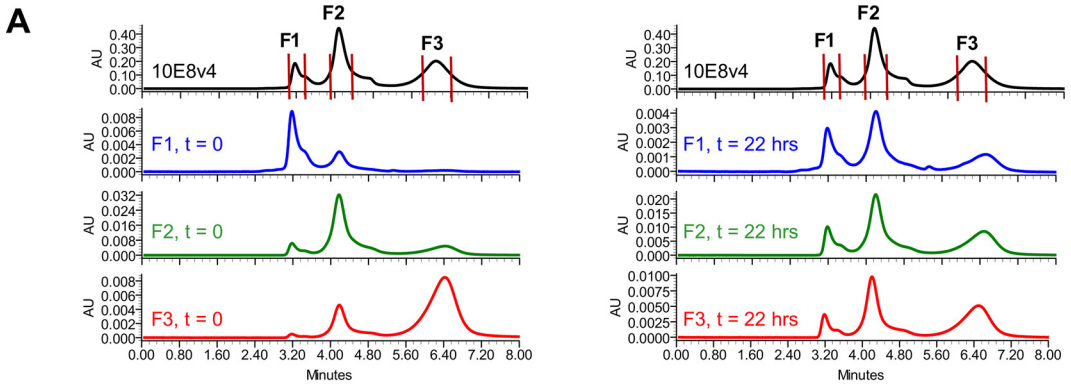

MW by MALS

mAb / Peak Number	F1	F2	F3
VRC01	150	-----	-----
10E8v4	143	129	150

C

IC50 (μg/ml)

Clade	Virus	10E8v4	10E8v4-DS
A	KER2008.12.SG3	>50	>50
ACD	6095.V1.C10.SG3	0.004	0.002
AE	TH966.8.SG3	0.026	0.092
B	6101.10.SG3	0.011	2.410
B	PVO.04.SG3	0.894	2.530
B	YU2.DG.SG3	0.668	0.275
C	CNE31.SG3	1.740	2.280
C	ZM106.9.SG3	>50	>50
C	ZM215.8.SG3	0.042	0.208
	Median IC50	0.042	0.275
	Geometric Mean	0.091	0.283

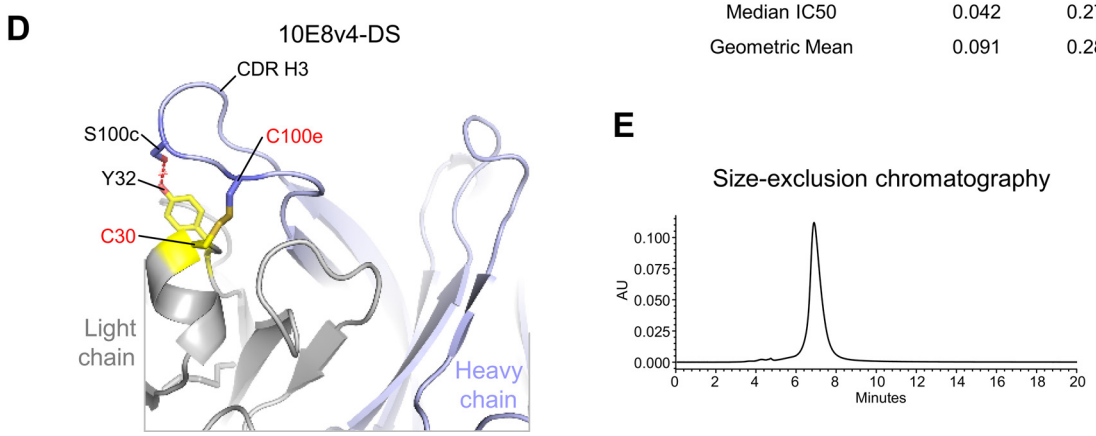

FIG 11 Size exclusion chromatography anomaly resulted from slow conformational isomerization, which an engineered disulfide resolves. (A) Size exclusion chromatography showed 10E8v4 to elute as three peaks (top chromatogram); when each fraction was immediately reinjected, it eluted as a mostly single peak (left chromatograms). However, if each of the separated peaks was allowed to equilibrate for 22 h, each now isomerized into three peaks (right chromatograms). (B) Multiangle light scattering (SEC-MALS) analysis. MW, molecular weight in thousands. (C) Neutralization potency of 10E8v4 and 10E8v4-DS. (D) An engineered disulfide between residue 100e on the heavy chain and residue 30 on the light chain to prevent isomerization. (E) 10E8v4 with an interchain disulfide, 100eC-30C (DS), eluted as a single peak in size exclusion chromatography.

efficacious dose of 10E8v4 (or 10E8v4-DS) required *in vivo* to inhibit HIV-1, whether such a dose can be practically delivered by subcutaneous injection, and the degree to which additional surface alteration might improve 10E8v4 potency.

ACKNOWLEDGMENTS

We thank C. Soto for assistance with sequence deposition, J. Stuckey for assistance with figures, and members of the Structural Biology Section and Structural Bioinformatics Core, Vaccine Research Center, for discussions and comments on the manuscript.

Support for this work was provided by the U.S. National Institutes of Health Intramural Research Program (Vaccine Research Center, National Institute of Allergy and Infectious Diseases) and by the Bill and Melinda Gates Foundation Collaboration for AIDS Vaccine Discovery (OPP1039775 to J.R.M. and P.D.K.). Use of insertion device 22 (SER-CAT) at the Advanced Photon Source was supported by the U.S.

Department of Energy, Basic Energy Sciences, Office of Science, under contract W-31-109-Eng-38.

FUNDING INFORMATION

This work, including the efforts of John R. Mascola and Peter D. Kwong, was funded by Bill and Melinda Gates Foundation (OPP1039775). This work, including the efforts of Peter D. Kwong, was funded by Intramural Research Program, Vaccine Research Center, National Institute of Allergy and Infectious Diseases (VRC, NIAID) (ZIA AI005022-15).

REFERENCES

1. **Corti D, Langedijk JPM, Hinz A, Seaman MS, Vanzetta F, Fernandez-Rodriguez BM, Silacci C, Pinna D, Jarrossay D, Balla-Jhagjhoorsingh S, Willems B, Zekveld MJ, Dreja H, O'Sullivan E, Pade C, Orkin C, Jeffs SA, Montefiori DC, Davis D, Weissenhorn W, McKnight A, Heeney JL, Sallusto F, Sattentau QJ, Weiss RA, Lanzavecchia A.** 2010. Analysis of memory B cell responses and isolation of novel monoclonal antibodies with neutralizing breadth from HIV-1-infected individuals. PLoS One **5:**e8805. http://dx.doi.org/10.1371/journal.pone.0008805.
2. **Doria-Rose NA, Schramm CA, Gorman J, Moore PL, Bhiman JN, DeKosky BJ, Ernandes MJ, Georgiev IS, Kim HJ, Pancera M, Staupe RP, Altae-Tran HR, Bailer RT, Crooks ET, Cupo A, Druz A, Garrett NJ, Hoi KH, Kong R, Louder MK, Longo NS, McKee K, Nonyane M, O'Dell S, Roark RS, Rudicell RS, Schmidt SD, Sheward DJ, Soto C, Wibmer CK, Yang YP, Zhang ZH, Mullikin JC, Binley JM, Sanders RW, Wilson IA, Moore JP, Ward AB, Georgiou G, Williamson C, Karim SSA, Morris L, Kwong PD, Shapiro L, Mascola JR.** 2014. Developmental pathway for potent V1V2-directed HIV-neutralizing antibodies. Nature **509:**55–62. http://dx.doi.org/10.1038/nature13036.
3. **Falkowska E, Le KM, Ramos A, Doores KJ, Lee JH, Blattner C, Ramirez A, Derking R, MJ van Gils Liang CH, Mcbride R, von Bredow B, Shivatare SS, Wu CY, Chan-Hui PY, Liu Y, Feizi T, Zwick MB, Koff WC, Seaman MS, Swiderek K, Moore JP, Evans D, Paulson JC, Wong CH, Ward AB, Wilson IA, Sanders RW, Poignard P, Burton DR.** 2014. Broadly neutralizing HIV antibodies define a glycan-dependent epitope on the prefusion conformation of gp41 on cleaved envelope trimers. Immunity **40:**657–668. http://dx.doi.org/10.1016/j.immuni.2014.04.009.
4. **Huang JH, Kang BH, Pancera M, Lee JH, Tong T, Feng Y, Imamichi H, Georgiev IS, Chuang GY, Druz A, Doria-Rose NA, Laub L, Sliepen K, van Gils MJ, de la Pena AT, Derking R, Klasse PJ, Migueles SA, Bailer RT, Alam M, Pugach P, Haynes BF, Wyatt RT, Sanders RW, Binley JM, Ward AB, Mascola JR, Kwong PD, Connors M.** 2014. Broad and potent HIV-1 neutralization by a human antibody that binds the gp41-gp120 interface. Nature **515:**138–142. http://dx.doi.org/10.1038/nature13601.
5. **Kwong PD, Mascola JR.** 2012. Human antibodies that neutralize HIV-1: identification, structures, and B cell ontogenies. Immunity **37:**412–425. http://dx.doi.org/10.1016/j.immuni.2012.08.012.
6. **Sok D, van Gils MJ, Pauthner M, Julien JP, Saye-Francisco KL, Hsueh J, Briney B, Lee JH, Le KM, Lee PS, Hua YZ, Seaman MS, Moore JP, Ward AB, Wilson IA, Sanders RW, Burton DR.** 2014. Recombinant HIV envelope trimer selects for quaternary-dependent antibodies targeting the trimer apex. Proc Natl Acad Sci U S A **111:**17624–17629. http://dx.doi.org/10.1073/pnas.1415789111.
7. **Walker LM, Huber M, Doores KJ, Falkowska E, Pejchal R, Julien JP, Wang SK, Ramos A, Chan-Hui PY, Moyle M, Mitcham JL, Hammond PW, Olsen OA, Phung P, Fling S, Wong CH, Phogat S, Wrin T, Simek MD, Koff WC, Wilson IA, Burton DR, Poignard P.** 2011. Broad neutralization coverage of HIV by multiple highly potent antibodies. Nature **477:**466–470. http://dx.doi.org/10.1038/nature10373.
8. **Wu XL, Yang ZY, Li YX, Hogerkorp CM, Schief WR, Seaman MS, Zhou TQ, Schmidt SD, Wu L, Xu L, Longo NS, McKee K, O'Dell S, Louder MK, Wycuff DL, Feng Y, Nason M, Doria-Rose N, Connors M, Kwong PD, Roederer M, Wyatt RT, Nabel GJ, Mascola JR.** 2010. Rational design of envelope identifies broadly neutralizing human monoclonal antibodies to HIV-1. Science **329:**856–861. http://dx.doi.org/10.1126/science.1187659.
9. **Zhou TQ, Georgiev I, Wu XL, Yang ZY, Dai KF, Finzi A, Kwon YD, Scheid JF, Shi W, Xu L, Yang YP, Zhu JA, Nussenzweig MC, Sodroski J, Shapiro L, Nabel GJ, Mascola JR, Kwong PD.** 2010. Structural basis for broad and potent neutralization of HIV-1 by antibody VRC01. Science **329:**811–817. http://dx.doi.org/10.1126/science.1192819.
10. **Barouch DH, Whitney JB, Moldt B, Klein F, Oliveira TY, Liu J, Stephenson KE, Chang HW, Shekhar K, Gupta S, Nkolola JP, Seaman MS, Smith KM, Borducchi EN, Cabral C, Smith JY, Blackmore S, Sanisetty S, Perry JR, Beck M, Lewis MG, Rinaldi W, Chakraborty AK, Poignard P, Nussenzweig MC, Burton DR.** 2013. Therapeutic efficacy of potent neutralizing HIV-1-specific monoclonal antibodies in SHIV-infected rhesus monkeys. Nature **503:**224–228. http://dx.doi.org/10.1038/nature12744.
11. **Caskey M, Klein F, Lorenzi JCC, Seaman MS, West AP, Buckley N, Kremer G, Nogueira L, Braunschweig M, Scheid JF, Horwitz JA, Shimeliovich I, Ben-Avraham S, Witmer-Pack M, Platten M, Lehmann C, Burke LA, Hawthorne T, Gorelick RJ, Walker BD, Keler T, Gulick RM, Fatkenheuer G, Schlesinger SJ, Nussenzweig MC.** 2015. Viraemia suppressed in HIV-1-infected humans by broadly neutralizing antibody 3BNC117. Nature **522:**487–491. http://dx.doi.org/10.1038/nature14411.
12. **Mascola JR.** 2002. Passive transfer studies to elucidate the role of antibody-mediated protection against HIV-1. Vaccine **20:**1922–1925. http://dx.doi.org/10.1016/S0264-410X(02)00068-3.
13. **Voronin Y, Mofenson LM, Cunningham CK, Fowler MG, Kaleebu P, McFarland EJ, Safrit JT, Graham BS, Snow W.** 2014. HIV monoclonal antibodies: a new opportunity to further reduce mother-to-child HIV transmission. Plos Med **11:**e1001616. http://dx.doi.org/10.1371/journal.pmed.1001616.
14. **Huang JH, Ofek G, Laub L, Louder MK, Doria-Rose NA, Longo NS, Imamichi H, Bailer RT, Chakrabarti B, Sharma SK, Alam SM, Wang T, Yang YP, Zhang BS, Migueles SA, Wyatt R, Haynes BF, Kwong PD, Mascola JR, Connors M.** 2012. Broad and potent neutralization of HIV-1 by a gp41-specific human antibody. Nature **491:**406–412. http://dx.doi.org/10.1038/nature11544.
15. **Lee JH, Ozorowski G, Ward AB.** 2016. Cryo-EM structure of a native, fully glycosylated, cleaved HIV-1 envelope trimer. Science **351:**1043–1048. http://dx.doi.org/10.1126/science.aad2450.
16. **Cardoso RMF, Zwick MB, Stanfield RL, Kunert R, Binley JM, Katinger H, Burton DR, Wilson IA.** 2005. Broadly neutralizing anti-HIV antibody 4E10 recognizes a helical conformation of a highly conserved fusion-associated motif in gp41. Immunity **22:**163–173. http://dx.doi.org/10.1016/j.immuni.2004.12.011.
17. **Zwick MB, Jensen R, Church S, Wang M, Stiegler G, Kunert R, Katinger H, Burton DR.** 2005. Anti-human immunodeficiency virus type 1 (HIV-1) antibodies 2F5 and 4E10 require surprisingly few crucial residues in the membrane-proximal external region of glycoprotein gp41 to neutralize HIV-1. J Virol **79:**1252–1261. http://dx.doi.org/10.1128/JVI.79.2.1252-1261.2005.
18. **Zwick MB, Labrijn AF, Wang M, Spenlehauer C, Saphire EO, Binley JM, Moore JP, Stiegler G, Katinger H, Burton DR, Parren PWHI.** 2001. Broadly neutralizing antibodies targeted to the membrane-proximal external region of human immunodeficiency virus type 1 glycoprotein gp41. J Virol **75:**10892–10905. http://dx.doi.org/10.1128/JVI.75.22.10892-10905.2001.
19. **Kabsch W, Sander C.** 1983. Dictionary of protein secondary structure—pattern-recognition of hydrogen-bonded and geometrical features. Biopolymers **22:**2577–2637. http://dx.doi.org/10.1002/bip.360221211.
20. **Gainza P, Roberts KE, Georgiev I, Lilien RH, Keedy DA, Chen CY, Reza F, Anderson AC, Richardson DC, Richardson JS, Donald BR.** 2013. OSPREY: protein design with ensembles, flexibility, and provable algorithms. Methods Protein Design **523:**87–107. http://dx.doi.org/10.1016/B978-0-12-394292-0.00005-9.
21. **Sarzotti-Kelsoe M, Bailer RT, Turk E, Lin CL, Bilska M, Greene KM, Gao HM, Todd CA, Ozaki DA, Seaman MS, Mascola JR, Montefiori DC.** 2014. Optimization and validation of the TZM-bl assay for standardized assessments of neutralizing antibodies against HIV-1. J Immunol Methods **409:**131–146. http://dx.doi.org/10.1016/j.jim.2013.11.022.
22. **Rudicell RS, Do Kwon Y, Ko SY, Pegu A, Louder MK, Georgiev IS, Wu XL, Zhu J, Boyington JC, Chen XJ, Shi W, Yang ZY, Doria-Rose NA, McKee K, O'Dell S, Schmidt SD, Chuang GY, Druz A, Soto C, Yang YP, Zhang BS, Zhou TQ, Todd JP, Lloyd KE, Eudailey J, Roberts KE, Donald BR, Bailer RT, Ledgerwood J, Mullikin JC, Shapiro L, Koup RA, Graham BS, Nason MC, Connors M, Haynes BF, Rao SS, Roederer M, Kwong PD, Mascola JR, Nabel GJ.** 2014. Enhanced potency of a broadly neutralizing HIV-1 antibody *in vitro* improves protection against lentiviral infection *in vivo*. J Virol **88:**12669–12682. http://dx.doi.org/10.1128/JVI.02213-14.
23. **Majeed S, Ofek G, Belachew A, Huang CC, Zhou TQ, Kwong PD.** 2003.

Enhancing protein crystallization through precipitant synergy. Structure **11:**1061–1070. http://dx.doi.org/10.1016/S0969-2126(03)00185-0.

24. **Otwinowski Z, Minor W.** 1997. Processing of X-ray diffraction data collected in oscillation mode. Macromol Crystallogr Part A **276:**307–326. http://dx.doi.org/10.1016/S0076-6879(97)76066-X.
25. **McCoy AJ, Grosse-Kunstleve RW, Adams PD, Winn MD, Storoni LC, Read RJ.** 2007. Phaser crystallographic software. J Appl Crystallogr **40:** 658–674. http://dx.doi.org/10.1107/S0021889807021206.
26. **Adams PD, Afonine PV, Bunkoczi G, Chen VB, Davis IW, Echols N, Headd JJ, Hung LW, Kapral GJ, Grosse-Kunstleve RW, McCoy AJ, Moriarty NW, Oeffner R, Read RJ, Richardson DC, Richardson JS, Terwilliger TC, Zwart PH.** 2010. PHENIX: a comprehensive Python-based system for macromolecular structure solution. Acta Crystallogr D Biol Crystallogr **66:**213–221. http://dx.doi.org/10.1107/S0907444909052925.
27. **Emsley P, Cowtan K.** 2004. Coot: model-building tools for molecular graphics. Acta Crystallogr D Biol Crystallogr **60:**2126–2132. http://dx.doi.org/10.1107/S0907444904019158.
28. **Cardoso RMF, Brunel FM, Ferguson S, Zwick M, Burton DR, Dawson PE, Wilson IA.** 2007. Structural basis of enhanced binding of extended and helically constrained peptide epitopes of the broadly neutralizing HIV-1 antibody 4E10. J Mol Biol **365:**1533–1544. http://dx.doi.org/10.1016/j.jmb.2006.10.088.
29. **Chen J, Frey G, Peng H, Rits-Volloch S, Garrity J, Seaman MS, Chen B.** 2014. Mechanism of HIV-1 neutralization by antibodies targeting a membrane-proximal region of gp41. J Virol **88:**1249–1258. http://dx.doi.org/10.1128/JVI.02664-13.
30. **Julien JP, Huarte N, Maeso R, Taneva SG, Cunningham A, Nieva JL, Pai EF.** 2010. Ablation of the complementarity-determining region H3 apex of the anti-HIV-1 broadly neutralizing antibody 2F5 abrogates neutralizing capacity without affecting core epitope binding. J Virol **84:**4136–4147. http://dx.doi.org/10.1128/JVI.02357-09.
31. **Kim M, Sun ZYJ, Rand KD, Shi XM, Song LK, Cheng YX, Fahmy AF, Majumdar S, Ofek G, Yang YP, Kwong PD, Wang JH, Engen JR, Wagner G, Reinherz EL.** 2011. Antibody mechanics on a membrane-bound HIV segment essential for GP41-targeted viral neutralization. Nat Struct Mol Biol **18:**1235–1243. http://dx.doi.org/10.1038/nsmb.2154.
32. **Ofek G, McKee K, Yang YP, Yang ZY, Skinner J, Guenaga FJ, Wyatt R, Zwick MB, Nabel GJ, Mascola JR, Kwong PD.** 2010. Relationship between antibody 2F5 neutralization of HIV-1 and hydrophobicity of its heavy chain third complementarity-determining region. J Virol **84:**2955–2962. http://dx.doi.org/10.1128/JVI.02257-09.
33. **Ofek G, Tang M, Sambor A, Katinger H, Mascola JR, Wyatt R, Kwong PD.** 2004. Structure and mechanistic analysis of the anti-human immunodeficiency virus type 1 antibody 2F5 in complex with its gp41 epitope. J Virol **78:**10724–10737. http://dx.doi.org/10.1128/JVI.78.19.10724-10737.2004.
34. **Ofek G, Zirkle B, Yang YP, Zhu ZY, McKee K, Zhang BS, Chuang GY, Georgiev IS, O'Dell S, Doria-Rose N, Mascola JR, Dimitrov DS, Kwong PD.** 2014. Structural basis for HIV-1 neutralization by 2F5-like antibodies m66 and m66.6. J Virol **88:**2426–2441. http://dx.doi.org/10.1128/JVI.02837-13.
35. **Sun ZYJ, Oh KJ, Kim MY, Yu J, Brusic V, Song LK, Qiao ZS, Wang JH, Wagner G, Reinherz EL.** 2008. HIV-1 broadly neutralizing antibody extracts its epitope from a kinked gp41 ectodomain region on the viral membrane. Immunity **28:**52–63. http://dx.doi.org/10.1016/j.immuni.2007.11.018.
36. **Georgiev IS, Rudicell RS, Saunders KO, Shi W, Kirys T, McKee K, O'Dell S, Chuang GY, Yang ZY, Ofek G, Connors M, Mascola JR, Nabel GJ, Kwong PD.** 2014. Antibodies VRC01 and 10E8 neutralize HIV-1 with high breadth and potency even with Ig-framework regions substantially reverted to germline. J Immunol **192:**1100–1106. http://dx.doi.org/10.4049/jimmunol.1302515.
37. **Zhu J, Ofek G, Yang YP, Zhang BS, Louder MK, Lu G, McKee K, Pancera M, Skinner J, Zhang ZH, Parks R, Eudailey J, Lloyd KE, Blinn J, Alam SM, Haynes BF, Simek M, Burton DR, Koff WC, Mullikin JC, Mascola JR, Shapiro L, Kwong PD.** 2013. Mining the antibodyome for HIV-1-neutralizing antibodies with next-generation sequencing and phylogenetic pairing of heavy/light chains. Proc Natl Acad Sci U S A **110:** 6470–6475. http://dx.doi.org/10.1073/pnas.1219320110.
38. **Ko SY, Pegu A, Rudicell RS, Yang ZY, Joyce MG, Chen XJ, Wang KY, Bao S, Kraemer TD, Rath T, Zeng M, Schmidt SD, Todd JP, Penzak SR, Saunders KO, Nason MC, Haase AT, Rao SS, Blumberg RS, Mascola JR, Nabel GJ.** 2014. Enhanced neonatal Fc receptor function improves protection against primate SHIV infection. Nature **514:**642–645. http://dx.doi.org/10.1038/nature13612.
39. **Zalevsky J, Chamberlain AK, Horton HM, Karki S, Leung IW, Sproule TJ, Lazar GA, Roopenian DC, Desjarlais JR.** 2010. Enhanced antibody half-life improves in vivo activity. Nat Biotechnol **28:**157–159. http://dx.doi.org/10.1038/nbt.1601.
40. **Pegu A, Yang ZY, Boyington JC, Wu L, Ko SY, Schmidt SD, McKee K, Kong WP, Shi W, Chen XJ, Todd JP, Letvin NL, Huang JH, Nason MC, Hoxie JA, Kwong PD, Connors M, Rao SS, Mascola JR, Nabel GJ.** 2014. Neutralizing antibodies to HIV-1 envelope protect more effectively in vivo than those to the CD4 receptor. Sci Transl Med **6:**243ra88. http://dx.doi.org/10.1126/scitranslmed.3008992.
41. **Ledgerwood JE, Coates EE, Yamshchikov G, Saunders JG, Holman L, Enama ME, DeZure A, Lynch RM, Gordon I, Plummer S, Hendel CS, Pegu A, Conan-Cibotti M, Sitar S, Bailer RT, Narpala S, McDermott A, Louder M, O'Dell S, Mohan S, Pandey JP, Schwartz RM, Hu Z, Koup RA, Capparelli E, Mascola JR, Graham BS.** 2015. Safety, pharmacokinetics and neutralization of the broadly neutralizing HIV-1 human monoclonal antibody VRC01 in healthy adults. Clin Exp Immunol **182:**289–301. http://dx.doi.org/10.1111/cei.12692.
42. **Lynch RM, Boritz E, Coates EE, DeZure A, Madden P, Costner P, Enama ME, Plummer S, Holman L, Hendel CS, Gordon I, Casazza J, Conan-Cibotti M, Migueles SA, Tressler R, Bailer RT, McDermott A, Narpala S, O'Dell S, Wolf G, Lifson JD, Freemire BA, Gorelick RJ, Pandey JP, Mohan S, Chomont N, Fromentin R, Chun TW, Fauci AS, Schwartz RM, Koup RA, Douek DC, Hu Z, Capparelli E, Graham BS, Mascola JR, Ledgerwood JE.** 2015. Virologic effects of broadly neutralizing antibody VRC01 administration during chronic HIV-1 infection. Sci Transl Med **7:**319ra206. http://dx.doi.org/10.1126/scitranslmed.aad5752.
43. **Meffre E, Catalan N, Seltz F, Fischer A, Nussenzweig MC, Durandy A.** 2001. Somatic hypermutation shapes the antibody repertoire of memory B cells in humans. J Exp Med **194:**375–378. http://dx.doi.org/10.1084/jem.194.3.375.
44. **Wu XL, Zhang ZH, Schramm CA, Joyce MG, Do Kwon Y, Zhou TQ, Sheng ZZ, Zhang BS, O'Dell S, McKee K, Georgiev IS, Chuang GY, Longo NS, Lynch RM, Saunders KO, Soto C, Srivatsan S, Yang YP, Bailer RT, Louder MK, Mullikin JC, Connors M, Kwong PD, Mascola JR, Shapiro L.** 2015. Maturation and diversity of the VRC01-antibody lineage over 15 years of chronic HIV-1 infection. Cell **161:**470–485. http://dx.doi.org/10.1016/j.cell.2015.03.004.